

Christian Hellmich¹

Institute for Mechanics of Materials and Structures,
TU Wien (Vienna University of Technology),
Vienna 1040, Austria
e-mail: christian.hellmich@tuwien.ac.at

Niketa Ukaj

Institute for Mechanics of Materials and Structures,
TU Wien (Vienna University of Technology),
Vienna 1040, Austria
e-mail: niketa.ukaj@tuwien.ac.at

Bart Smeets

Biomechanics Section,
Department of Mechanical Engineering,
KU Leuven,
Leuven 3001, Belgium
e-mail: bart.smeets@kuleuven.be

Hans van Oosterwyck

Biomechanics Section,
Department of Mechanical Engineering,
KU Leuven,
Leuven 3001, Belgium
e-mail: hans.vanoosterwyck@kuleuven.be

Nenad Filipovic

Faculty of Engineering,
University of Kragujevac,
Kragujevac 34000, Serbia
e-mail: fica@kg.ac.rs

Luis Zelaya-Lainez

Institute for Mechanics of Materials and Structures,
TU Wien (Vienna University of Technology),
Vienna 1040, Austria
e-mail: luis.zelaya@tuwien.ac.at

Johannes Kalliauer

Institute for Mechanics of Materials and Structures,
TU Wien (Vienna University of Technology),
Vienna 1040, Austria
e-mail: johannes.kalliauer@tuwien.ac.at

Stefan Scheiner

Institute for Mechanics of Materials and Structures,
TU Wien (Vienna University of Technology),
Vienna 1040, Austria
e-mail: stefan.scheiner@tuwien.ac.at

Hierarchical Biomechanics: Concepts, Bone as Prominent Example, and Perspectives Beyond

The main motivation for “hierarchical biomechanics” is that the wide variability of mechanical properties encountered at the macroscopic scale may be traced back to just a few “universal” or invariant mechanical properties of elementary components at a sufficiently small scale (such as collagen, elastin, and water in case of soft tissues; complemented by hydroxyapatite in case of hard “mineralized” tissues such as bone), and to the nano- and microstructures which the latter build up. This challenging task requires a physically rigorous and mathematically sound basis, as provided by Finite Element and Fast Fourier Transform methods, as well as by continuum micromechanics resting on (semi-)analytical solutions for Eshelby-type matrix-inclusion problems. Corresponding numerical and analytical mathematical models have undergone diligent experimental validation, by means of data stemming from a variety of biophysical, biochemical, and biomechanical testing methods, such as light and electron microscopy, ultrasonic testing, and scanning acoustic microscopy, as well as physicochemical tests associated with dehydration, demineralization, decollagenization, ashing, and weighing in air and fluid. While elastic scale transition and homogenization methods have attained a high maturity level, the hierarchical nature of dissipative (i.e., viscous or strength) properties is still a vibrant field of research. This applies even more to hierarchical approaches elucidating the interface between biological cells and extracellular matrices (“mechanobiology”), to cells interacting in complex biofluids such as blood, and to the intricate and highly undiscovered mechanics unfolding within biological cells. [DOI: 10.1115/1.4055032]

1 Introduction—Scope

In an interesting, recently published review article, Alber et al. [1] propose the following definition of *multiscale modeling*: “*Multiscale modeling is a successful strategy to integrate multiscale, multiphysics data and uncover mechanisms that explain the*

emergence of function.” In this context, Alber et al. [1] refer to “small-scale” constitutive equations, and “large-scale” conservation laws as the general physical frame in which the multiscale models, being themselves supported by machine learning if necessary, may be developed. Thereby, the small-scale constitutive equations may be adopted from the classical engineering field, by considering elastic, viscoelastic, or elastoplastic behavior. As concerns living materials, the constitutive equations may be more complex, and concerning the “large-scale laws”, biological applications may require rethinking “of the underlying kinetics, the

¹Corresponding author.

Manuscript received October 29, 2021; final manuscript received July 13, 2022; published online August 16, 2022. Assoc. Editor: Thomas Siegmund.

balance of mass, and the laws of thermodynamics”, and also the inclusion of “the biological, chemical, or electrical fields that act as stimuli of this living response”. We here embrace the aforementioned focus on integration of multiscale/multiphysics data, and we share with Alber et al. [1] a deep root in engineering mechanics, as evidenced through their association of small-scale differential equations with classical mechanical behaviors, such as elasticity [2], viscoelasticity [3,4], and elastoplasticity [5,6]. Accordingly, we set, in this review paper, the primary focus on multiscale mechanics modeling. This choice appears natural, given the importance of mechanics-related aspects in the biomedical field, in particular when focusing on multiscale modeling. However, we wish to complement the account of the state of the art by Alber et al. [1] in multiscale modeling of biomedical materials and systems, by adopting an extended theoretical frame. More specifically, we set our focus not so much on *one* small (“constitutive”) versus *one* large (“conservation laws-related”) scale, but on the numerous intermediate scales, where one type of constitutive behavior is effectively transformed into another type of constitutive behavior. At the same time, we wish to review and discuss how the constitutive behavior at the smallest relevant scale of a biomechanical system may be either governed by largely invariant (“universal”) continuum mechanical properties, or even from atomistic mechanics, in both cases avoiding any empirical parameter fitting. It is this focus on the intermediate scales and on the corresponding successive scale transitions, which defines the (bio-)mechanical science-related literature reviewed and discussed in this paper, referred to by the term “hierarchical biomechanics”. Still, we do not restrict ourselves to multiscale methods for pure mechanics, but we also address the exploration of the cross-roads of mechanics/physics and biology, as it is well-known that biologically driven processes may influence mechanical properties, and that, in turn, mechanical loading may influence the biological environment. In this context, the present review is completed by multiscale modeling concepts which, in a theoretically consistent manner, obey both the traditions of mechanics/physics (by employing field theories, interaction/constitutive laws, and geometrical compatibility), and of biology (by employing cell population dynamics, and cell biology models).

2 The Representative Volume Element—“Home” of a Constitutive Law

2.1 Poromechanical Approach. As a rule, biomedical materials and biological tissues are hierarchically organized, encompassing multiple pore spaces and other organizational patterns at different length scales [7,8]. Therefore, the *ad hoc* adoption of the material point concept inherent to traditional solid mechanics is not straightforward, and in most cases even questionable. This suggests prudence and good reasoning whenever using standard continuum mechanics quantities associated with the so-called material point, such as the Cauchy stress tensor (and associated notions of mechanical strength), various types of strain tensors (in particular the Green–Lagrange or the linearized strain tensor), or corresponding stress–strain laws (also referred to as constitutive laws), in the context of highly complex biological and biomedical materials. A good starting point for tackling the corresponding challenges is to resort to well-accepted, theoretically formulated and practically useful concepts which originate from geotechnical engineering, and which actually form the very basis of the scientific field called poromechanics [9]—, i.e., mechanics of porous media, rather than mechanics of pure solids.

A conceptual crystallization point in this context is the so-called representative volume element (RVE), which may be traced back to Biot’s famous 1941 treatise on consolidation [10]—the latter is, in Biot’s words, a “*phenomenon [...] whose mechanism is known to be in many cases identical with the process of squeezing water out of an elastic porous medium.*” For the appropriate

representation of such an elastic porous medium, Biot proposes: “*Consider a small cubic element of the consolidating soil, its sides being parallel with the coordinate axes. This element is taken to be large enough compared to the size of the pores so that it may be treated as homogeneous, and at the same time small enough, compared to the scale of the macroscopic phenomena in which we are interested, so that it may be considered as infinitesimal in the mathematical treatment.*”

We see that Biot defines a small element, at the same time, both as a point at the macroscopic scale and as a volumetrically extended (here cubic) entity at the microscopic scale. Explicitly assigning two scales to one and the same element goes impressively beyond the material point concept of classical solid mechanics, and hence, is not only qualified as the birth of poromechanics, but, from a more general viewpoint, marks the actual starting point of multiscale modeling in the engineering sciences—long before this term eventually gained ubiquitous popularity, both in the traditional engineering sciences and beyond, especially so in biomedical engineering. The concept of such a simple RVE consisting of a solid matrix and a fluid-filled pore space entails a fundamentally new constitutive property. The latter is called Biot coefficient in the isotropic case [10], and Biot tensor (of second order) in the general anisotropic case [11], and it links pore pressure variations, under constant macroscopic strains, to macroscopic RVE-related stresses. The RVE-concept implies repeated introduction of one and the same type of material property, namely, at different length scales: Elastic properties are assigned to the solid matrix at the microscopic scale and to the overall porous medium, i.e., to the entire RVE. As an additional complication, the overall, RVE-related elastic properties depend again on the action of the fluid, with two important limit cases, as first described by Gassmann [12]: (i) the case of empty pores or of pores with pressures governed from outside of the RVE (drained stiffness), and (ii) the case of a closed RVE with the fluid being trapped inside the RVE (undrained conditions). Corresponding, meanwhile classical relations were applied to soils, rocks, and shales, and nurtured important technological progress in geotechnical and petroleum engineering throughout the next four decades. It was not before the late 1990s, that such basic poromechanical relations entered the bio-engineering realm. This was largely the merit of Cowin and coworkers, who dealt with the poroelasticity of bone [13,14], and transferred, very successfully, the consolidation problem into biomechanics, by discussing the role of fluid flow in stimulating biological cells residing in pores, one of the key topics of this review.

2.2 Micromechanical Approach. Independently of the early poromechanical developments, the idea of an RVE was also embraced by the community dealing with reinforced solids. Going beyond the poromechanicians’ conceptualization of a fluid pressure at the microscale, the reinforced solids community introduced the entire stress and strain fields at the microscale, thereby establishing, in the 1960s, a new scientific field called composite mechanics or continuum micromechanics [15]. The key concept of the latter is that a macroscopic material point is associated with a full continuum mechanics boundary value problem, formulated on an RVE defined at the microscopic scale. In terms of length scales, this RVE coincides with that of poromechanics. More specifically, the size of the pores is now taken by the size of any type of (solid) inhomogeneities, and the boundary of the RVE is subjected to a microscopic displacement field which is governed by homogeneous macroscopic strains. These boundary conditions readily imply a strain average rule [16,17]: The spatial average of kinematically compatible microscopic strains is equal to the macroscopic strain. Alternatively, if the boundary of the RVE is subjected to microscopic traction forces which are associated, via Cauchy’s fundamental theorem, with one and the same macroscopic stress tensor, the following stress average rule applies: The spatial average of equilibrated microscopic stresses is equal to the

macroscopic stress. Accordingly, one of the pioneers in the field, Rodney Hill, writes in 1963, when explaining what he calls “the representative volume” [16]: “*This phrase will be used when referring to a sample that (a) is structurally entirely typical of the whole mixture on average, and (b) contains a sufficient number of inclusions for the apparent overall moduli to be effectively independent of the surface values of traction and displacement, so long as these values are macroscopically uniform. That is, they fluctuate about a mean with a wavelength small compared with the dimensions of the sample, and the effects of such fluctuations become insignificant within a few wavelengths of the surface. The contribution of this surface layer to any average can be made negligible by taking the sample large enough.*” Hill has also complemented the stress and strain average rules by a third average rule associated with (rates of) work, standardly referred to as Hill’s lemma: The average (rate of) work done by equilibrated microstresses on kinematically compatible (rates of) microstrains is identical to the (rate of) work done by the macroscopic stresses on the macroscopic strains.

2.3 Representative Volume Element Size. In this context, the following practical question arises: Which ratio between the characteristic length of the RVE and that of the typical inhomogeneity within the RVE is needed to keep the aforementioned fluctuations sufficiently small, i.e., to make homogenization over microheterogeneity admissible and useful? This question had kept the scientific community busy for some time, until Drugan and Willis [18] provided a particularly satisfying answer, by considering the ergodicity principle and employing ensemble averaging. More precisely, Drugan and Willis [18] consider the RVE as an ergodic system where “*local configurations [of microscopic quantities, such as polarization stresses quantifying the fluctuation of elasticity tensors] occur over any one specimen with the frequency with which they occur over a single neighborhood in an ensemble of specimens.*” Hence, the spatial average of microstrains over one material sample representing the small material element in the sense of Biot and Hill becomes equivalent to the average of the microstrain at one specific microscopic point over an ensemble of very many samples representing the same type of material. Subsequent comparison of the mathematical solution for the stress–strain relations of the homogenized single sample with that of the ensemble averages reveals a surprising result: An RVE exceeding only twice the diameter of spherical reinforcements defining the microheterogeneity size already allows for an accurate prediction of the overall elasticity, as quantified by an error margin of only 5%. Only one year later, this somewhat surprising result was heuristically confirmed by Monte Carlo computations on cubic unit cells hosting very many different disordered arrangements of spheres subjected to periodic boundary conditions [19], and the same scale separation factor holds for parallel, infinitely long cylindrical inhomogeneities [20]. The rather small RVE size also indicates that the boundary of an RVE undergoing homogeneous (i.e., Hill-Hashin) boundary conditions must be carefully chosen: It needs to circumvent local environments with high elasticity fluctuations, as explicitly noted by Dormieux et al. [21] when discussing pores as “zero-stiffness reinforcements”.

2.4 Applications in Bio-Engineering. The aforementioned compact RVE sizes impressively underline the role of continuum (micro-)mechanics as a particularly efficient, robust, and versatile tool for materials with pronounced microscopic organizations, such as biological tissues. However, similar to the situation with poromechanical theories, RVE approaches hardly entered the biomedical field before the 1990s, and it was not before the 2000s until they started to flourish. They did particularly well for the intricate hierarchical organization of bone tissue where classical anatomical terms could be well assigned to RVEs of different sizes: trabecular bone to an RVE with a size of several millimeters [22–30], cortical bone to an RVE with a size of several hundred

micrometers [20,23,31–46], extravascular bone material to an RVE with a size of hundred micrometers [35,46,47], extracellular material to an RVE with a size of tens of micrometers [32,35,39,41,47–51], and finally both mineralized collagen fibrils [34,35,47,48,52–54] and extrafibrillar polycrystals [34,35,47,52,55] were assigned to RVEs with a size of about hundred nanometers. The latter two RVE types contain the elementary building blocks (or “major components” [7]) of bone: i.e., nanometer-sized hydroxyapatite crystals and crosslinked type I collagen molecules [52]. Notably, when using semi-analytical approaches, as discussed in more detail in Sec. 3, several of the aforementioned RVEs were straightforwardly combined to multistep homogenization schemes, sometimes referred to as “Russian doll models” [23,24,32,34,35,39,41,48–50,56–67]. In this case, the microheterogeneities within an RVE are represented by yet smaller RVEs, with the size of the latter being smaller or equal to the aforementioned microheterogeneity size [47]. An illustrative example is depicted in Fig. 1, featuring the hierarchical organization of cortical bone, from the macroscopic, structural scale down to the scale of single collagen molecules, hydroxyapatite crystals, and fluid-filled pore spaces, together with the corresponding multistep micromechanical representation. Again, the actual realization of homogeneous stress or strain boundary conditions imposed onto a sufficiently RVE may practically imply carefully chosen, somewhat wavy RVE boundaries deviating from Biot’s originally envisioned element (being of cubic shape), as can be seen from Level 5 shown in Fig. 1.

While bone appears as the most intensively studied biological tissue, several other biomedical materials have been studied by RVE approaches as well, including arterial wall tissue [73,74], muscle tissue [75], skin tissue [76–78], heart tissue [79], dentin [80–82], lung tissue [83,84], or synthetic tissue engineering materials [85–90].

The general nature and usefulness of the RVE being set now, it is time to continue with connecting microscopic to macroscopic physical quantities i.e., with scale transition: upscaling and downscaling.

3 Scale Transition—Up/Downscaling and Homogenization

3.1 The Classical Computational Mechanics Approach: Finite Element Method. The quest for efficient and/or accurate solutions for microscopic boundary value problems associated with RVEs has stirred enormous scientific efforts and led to many applications of standard computational mechanics-based approximation tools, such as the Finite Element (FE) method [20,29,76,83,85–94]. In the latter context, periodic boundary conditions are usually prescribed in a detailed representation of the RVE’s microstructure. The latter may be (i) geometrically well-defined, as is the case for synthetic tissue engineering scaffolds [85–87,89,90]; (ii) generated through suitable algorithms imitating key morphological features, such as fractal trees in skin microvasculature [76] or hexagonal staggered prisms in dental enamel [91]; or (iii) reconstructed from imaging data provided by techniques such as scanning acoustic microscopy [20,95] or microcomputed tomography (micro-CT) [29,83,88,92–94,96]. While appealing from a “ready-to-use” perspective which does not require deeper conceptual scrutiny, such approaches require a “full” description of the microstructure. Given the corresponding high computational demands, the latter are typically restricted to single-step homogenization procedures. Hence, the material properties entering the FE models on the integration point level either need to be known or suitably guessed, or they follow from additional, then analytical or semi-analytical homogenization and scale transition techniques “digging” deeper into the micro- and nanostructures of the investigated material systems [66,88,96].

3.2 Efficient Computational Strategies Based on Fast Fourier Transforms. With the FE method, the CPU time scales with the square of the degrees-of-freedom, which may render this

method inefficient for very large complex problems, where, in addition, meshing may become a challenge on its own. As a remedy, both the scaling and meshing problems can be elegantly overcome by numerical methods based on the Fast Fourier Transform (FFT). The latter methods rely on the smart use of Green's functions [97–99], i.e., of the solution for the displacement field

throughout an infinitely extended homogeneous elastic body subjected to a singular point load of unit intensity. First, the microheterogeneous linear elasticity field is equivalently represented as the superposition of a homogeneous elastic field and a field of microheterogeneous eigenstresses, so-called polarization stresses. Setting the microstress and microstrain fields of both

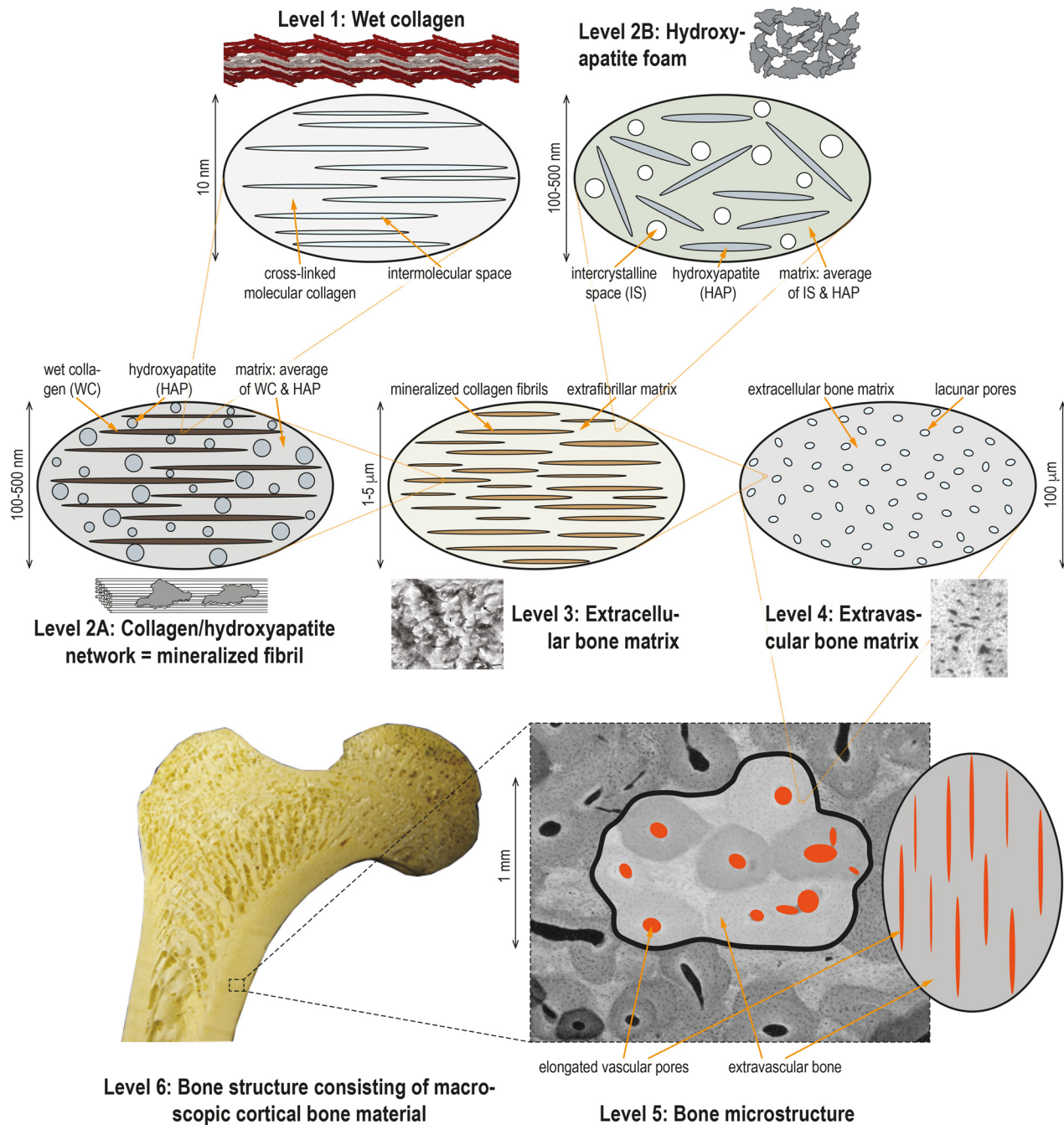


Fig. 1 Hierarchical organization of bone (see images and cartoons, respectively), and the corresponding micromechanical representation (elliptic cross sections through the three-dimensional RVEs), with indication of the respective characteristic lengths; the micromechanical representation follows from Refs. [35,47]. Note that on level 5, the region across which the representative volume is defined is precisely indicated (with the Haversian canals seen in their cross-sectional planes), whereas the respective cartoon is included as well (with the Haversian canals seen in longitudinal orientation). The image of wet collagen (level 1) is reprinted from Ref. [68], Copyright 2006 National Academy of Sciences, Washington, DC; the schematic images of the collagen/hydroxyapatite network (level 2A) and of the hydroxyapatite foam (level 2B) are reprinted from Ref. [35], with permission from Elsevier; the image of extracellular bone matrix (level 3) is reprinted by permission of Springer Nature Customer Service Center GmbH, from *Calcified Tissue International* [69], Copyright 1996; the image of extravascular bone matrix (level 4) is reprinted from Ref. [70], with permission from the Acoustic Society of America; the image of macroscopic bone material (level 5) is reprinted from Ref. [71], with permission of John Wiley & Sons, permission conveyed through Copyright Clearance Center, Inc.; and the image of the femoral whole bone structure (level 6) is reprinted from Ref. [72], with permission from Elsevier.

representations equal to each other delivers the polarization stresses as the tensor product of the microheterogeneous deviations of the micro-elasticity field from the properties of the homogeneous elastic body on the one hand, and the microstrains on the other hand [100–102]. This opens the way to incorporating solution schemes for the Lippmann-Schwinger equation—which was originally proposed in the framework of quantum mechanics [103]—into the conceptual framework of continuum micromechanics, particularly in the context of FFT analyses. The latter was pioneered by Moulinec and Suquet [104] and refined thereafter by Brisard and Dormieux [105]. Only very recently, namely, since 2018, these elegant solutions have made their way into the image-based micromechanics of cortical bone [38,67]. Such approaches outperform FE-based homogenization approaches by orders of magnitude in terms of computational efficiency—however, they still rely on “complete” microstructural information. This might be the reason why yet another approach, namely, that based on so-called material phases and estimates for homogenized mechanical properties, has gained much more popularity in the theoretical and applied mechanics field; and substantially propelled true multiscale approaches in biomechanics and bio-engineering.

3.3 Semi-Analytical Approaches Based on Elastic Matrix-Inhomogeneity Problems. The premise for phase-based estimation of RVE-related properties is the explicit awareness that the resolution of the microstructure in infinite completeness is eventually impossible. Accordingly, this resolution is not even aimed at, but the focus is a priori set at microstructural features potentially governing the homogenized mechanical behavior of the RVE. To that end, homogeneous subdomains, referred to as material phases, are introduced within the RVE [15,17,106]. Each material phase is characterized by homogeneous mechanical properties (such as a phase elasticity tensor, instead of a micro-elasticity

field), by a characteristic shape, and by the volume fraction it occupies within the RVE.

As the first key modeling step in phase-based homogenization, each phase is approximated by a homogeneous ellipsoidal elastic inhomogeneity, and each of those inclusions is embedded into the same type of infinitely extended auxiliary matrix subjected to homogeneous strains at its infinitely remote boundary, see Fig. 2. This auxiliary matrix exhibits elastic properties which are different from those of the inhomogeneity. The interest in such auxiliary matrix-inhomogeneity problems arises from the existence of corresponding analytical and semi-analytical solutions. They were provided by Eshelby [107] and by Laws [108], for inhomogeneities embedded in isotropic and anisotropic matrices, respectively. As was the case with the FFT solutions described in the last paragraph, also the solutions for Eshelby’s matrix-inhomogeneity problems were derived by combining the polarization stress concept with the method of Green’s functions. These solutions provide the remarkable result that the strains in the inhomogeneity are actually homogeneous and depend on the inhomogeneity shape, the elastic stiffness contrast between the inhomogeneity and the surrounding matrix, as well as on the remote matrix strains. If the investigated RVE is predominantly made up by a matrix phase in which inclusion phases are dilutely embedded, the RVE-related macroscopic strains can be approximated by the auxiliary matrix, and the macro-to-microstrain transition is already completed. Insertion of the phase strains into the phase-specific linear elastic laws yields phase stresses and averaging the latter over the RVE eventually gives access to macroscopic stresses; leading to the homogenized elasticity tensor associated with the so-called dilute homogenization scheme. Modeling of “dilute suspensions” can be traced back to Einstein’s 1906 treatment of rigid spherical inclusions in a Newtonian viscous fluid [109], and already appears as a broad review topic in Ref. [106].

However, for the frequently encountered cases where the individual phases are equally dominant in filling the RVE and

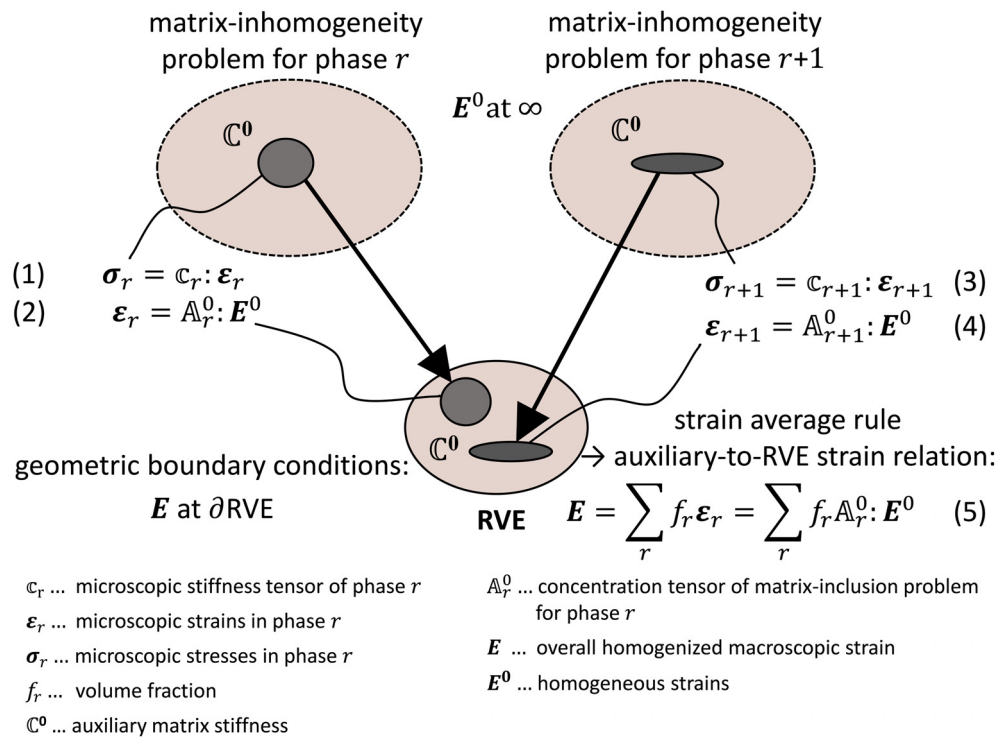


Fig. 2 Concept of matrix-inhomogeneity-problem-based homogenization (also called “mean-field-homogenization” or “homogenization of media with random microstructures”): several such problems are subjected to the same fictitious far-field strains, and then “superimposed” into an RVE, by means of the strain average rule; figure adapted and modified from Ref. [49], with permission of Elsevier

consequently interact with each other, a second key modeling step is necessary, as sketched by Mori and Tanaka in 1973 [110] and rigorously formulated by Benveniste in 1987 [111]: Namely, the matrix-inhomogeneity problems-related phase strains are inserted into the strain average rule, thereby providing a link between the remote auxiliary matrix strains and the macroscopic strains associated with the RVE, see Fig. 2. This link is then combined with the aforementioned solutions for the matrix-inhomogeneity problems, yielding relations between phase strains and RVE-related macroscopic strains. The latter relations are multilinear and hence expressed by so-called strain concentration or downscaling tensors of fourth order. Use of the phase-to-RVE strain relations in the phase-specific microscopic linear elastic law, and subsequent averaging of corresponding microstresses over the RVE yields the macroscopic (homogenized) RVE-related elasticity tensor, as an analytical or semi-analytical tensor function involving the elastic properties of the phases, their shapes, their volume fractions, and the stiffness of the auxiliary matrix [15], see also Fig. 3. Choice of

the latter completes the elasticity upscaling problem, with two main options: Choosing the matrix as an individual phase with given stiffness and volume fraction leads to the so-called Mori-Tanaka scheme [110], which is appropriate for matrix-inclusion composites. The second option is to assign the homogenized elastic properties and a zero volume fraction to the matrix. This leads to an implicit equation for the homogenized elastic properties. Its iterative solution is called self-consistent scheme. This scheme is appropriate for polycrystalline materials where all phases are in intimate mutual contact. Self-consistent schemes in the context of continuum mechanics can be traced back to the 1950s and 1960s [112–114]. However, they effectively entered bio-engineering only in the early 2000s, in the context of modeling the porous polycrystals (or mineral foams) [115] and the mineralized collagen fibrils [49] present in the ultrastructure of bone. From that time on, also the Mori-Tanaka homogenization scheme was successfully applied to various levels across the hierarchical organization of bone, namely, for the representation of wet collagen (Level 1 in

from Fig. 2: (2) → (1) → (5)		
macro-strain-to-micro-stress relation:	$\sigma_r = c_r : \mathbb{A}_r^0 : (\sum_r f_r \mathbb{A}_r^0)^{-1} : \mathbf{E}$	(i)
stress average rule:	$\Sigma = \sum_r \sigma_r$	(ii)
	Σ ... overall homogenized macroscopic stress	
(ii) → (i)	$\Sigma = \mathbb{C} : \mathbf{E}$	(iii)
	with $\mathbb{C} = \sum_r f_r c_r : \mathbb{A}_r^0 : (\sum_r f_r \mathbb{A}_r^0)^{-1}$	
	\mathbb{C} ... macroscopic (homogenized) elasticity tensor	
application to level 1:		
	$\mathbb{C}_{wetc} = \{(1 - f_{im}^{wetc}) \mathbb{C}_{col} + f_{im}^{wetc} \mathbb{C}_{im} : \mathbb{A}_{im}^{0,cyl}\} : \{(1 - f_{im}^{wetc}) \mathbb{I} + f_{im}^{wetc} \mathbb{A}_{im}^{0,cyl}\}^{-1}$	
application to level 2A:		
	$\mathbb{C}_{fib} = \{f_{wetc}^{fib} \mathbb{C}_{wetc} : \mathbb{A}_{wetc}^{0,cyl} + f_{HA}^{fib} \mathbb{C}_{HA} : \mathbb{A}_{HA}^{0,sph}\} : \{f_{wetc}^{fib} \mathbb{A}_{wetc}^{0,cyl} + f_{HA}^{fib} \mathbb{A}_{HA}^{0,sph}\}^{-1}$	
application to level 2B:		
	$\mathbb{C}_{ef} = \{f_{HA}^{ef} \mathbb{C}_{HA} : \int_{\varphi=0}^{2\pi} \int_{\vartheta=0}^{\pi} \mathbb{A}_{HA}^{0,cyl} \frac{\sin(\vartheta) d\vartheta d\varphi}{4\pi} + f_{ic}^{ef} \mathbb{C}_{ic} : \mathbb{A}_{ic}^{0,sph}\} :$ $\{f_{HA}^{ef} \int_{\varphi=0}^{2\pi} \int_{\vartheta=0}^{\pi} \mathbb{A}_{HA}^{0,cyl} \frac{\sin(\vartheta) d\vartheta d\varphi}{4\pi} + f_{ic}^{ef} \mathbb{A}_{ic}^{0,sph}\}^{-1}$	
application to level 3:		
	$\mathbb{C}_{ec} = \{(1 - f_{fib}^{ec}) \mathbb{C}_{ef} + f_{fib}^{ec} \mathbb{C}_{fib} : \mathbb{A}_{fib}^{0,cyl}\} : \{(1 - f_{fib}^{ec}) \mathbb{I} + f_{fib}^{ec} \mathbb{A}_{fib}^{0,cyl}\}^{-1}$	
application to level 4:		
	$\mathbb{C}_{ev} = \{f_{ec}^{ev} \mathbb{C}_{ec} + f_{lac}^{ev} \mathbb{C}_{lac} : \mathbb{A}_{lac}^{0,sph}\} : \{f_{ec}^{ev} \mathbb{I} + f_{lac}^{ev} \mathbb{A}_{lac}^{0,sph}\}^{-1}$	
application to level 5:		
	$\mathbb{C}_{micro} = \{(1 - f_{vas}^{micro}) \mathbb{C}_{ev} + f_{vas}^{micro} \mathbb{C}_{vas} : \mathbb{A}_{vas}^{0,cyl}\} : \{(1 - f_{vas}^{micro}) \mathbb{I} + f_{vas}^{micro} \mathbb{A}_{vas}^{0,cyl}\}^{-1}$	

Fig. 3 Stiffness homogenization over an RVE, based on the constitutive and concentration relations of Fig. 2; with application to the six RVEs depicted in Fig. 1; explicit expressions for the matrix inclusion problem-related concentration tensors can be found in Refs. [35,47]

Fig. 1), of the extracellular bone matrix (Level 3 in Fig. 1), of the extravascular bone matrix (Level 5 in Fig. 1), and of the macroscopic bone material (Level 6 in Fig. 1). The corresponding semi-analytical tensorial expressions are given in Fig. 3.

3.4 Semi-Analytical Approaches Based on Eigenstressed Matrix-Inhomogeneity Problems. Bio-engineering applications were a major driving force for developing Eshelby problem-based homogenization schemes for material properties beyond the elastic regime. The corresponding classical extension is that from elasticity to viscoelasticity, i.e., to assigning Boltzmann-type linear viscoelastic behavior to the material phases which *per se* remain fixed throughout time. In the Laplace-Carson space, such a linear viscoelastic behavior appears as a succession of formally linear elastic material behaviors, for each of which the classical Eshelby problem-based homogenization schemes described in the two preceding paragraphs can be employed, as explained in detail by Laws and McLaughlin in 1977 [116]. Effective application of this type of theory in bio-engineering took place only in 2014 [117], by assigning viscoelastic properties to the hydrated extrafibrillar mineral crystals in the ultrastructure of bone, in order to explain hydration- and mineralization-dependent creep of macroscopic bone material. In this context, the computational endeavors really start when back-transforming the homogenized properties into the time domain; e.g., by means of the Gaver-Wynn-Rho algorithm [118].

Another straightforward extension beyond elastic homogenization concerned perfectly brittle materials where failure at the microscopic level is directly associated with overall macroscopic failure of the RVE. Accordingly, the insertion of the phase stress-to-RVE stress relation (expressed by fourth-order stress concentration tensors) into a microscopic failure criterion directly yields a macroscopic failure criterion, which considers not only the strength properties of the weakest phase, but also the mechanical interaction of phases, driven by their shape, arrangement, and elastic stiffness contrast. However, when comparing the evaluation of corresponding mathematical formulations with experiments (see Sec. 4), the representation of the RVE's microstructure in terms of a finite number of phases generally turns out as a too crude approximation. As a remedy, the RVE may be represented by infinitely many nonspherical phases being oriented in all space directions, as indicated in Fig. 1, Level 2B, and labeled by polar and azimuthal angles [119]. Corresponding two-dimensional integrals over the unit sphere are then solved by appropriate approximation schemes such as Stroud's formulae [120]. This type of multiscale modeling has provided unprecedented insight into the strength characteristics of man-made hydroxyapatite biomaterials [121–123]—and more generally, of a large number of ceramic material systems [124,125].

However, what really broadens the application range of Eshelby-problem-based homogenization, is the explicit introduction of eigenstresses and eigenstrains in the true physical sense, i.e., the introduction of strains and/or stresses which are fully independent of elastic, i.e., nondissipative, phenomena. In the context of biomedical materials, two types of such eigen-quantities are of particular interest: plastic strains associated with ductile behavior, and pore pressures arising from fluids entering and leaving the various pore spaces found throughout the materials' hierarchical organizations. Important averaging rules for eigenstresses and eigenstrains go back to Levin [126] and follow from repeated use of Hill's lemma, as explained in Refs. [15,127]: The macroscopic eigenstress tensor is the average over the RVE, of the tensor contraction between the microscopic eigenstress tensor and the strain concentration tensor; and the macroscopic eigenstrain tensor is the average over the RVE, of the tensor contraction of the microscopic eigenstrain tensor and the stress concentration tensor. The aforementioned eigenstress averaging rule implies a most interesting link between the micromechanics of media with random microstructures and the classical

poroelasticity theory of Biot, as lined out in Ref. [21]: Considering a two-phase composite consisting of an elastic matrix and a pore space with eigenstresses of the format pore pressure times the second-order unity tensor yields the Biot tensor as the pore space-related strain concentration tensor times the porosity. This has a very important practical implication for the investigation of porous materials: The Biot tensors quantifying the interaction between pore pressure and macroscopic stress under a state free of macroscopic deformation need not be determined from complex poromechanical tests with independent control of pore pressure and macroscopic stress or strain, but can be readily determined once an elasticity homogenization scheme, as the ones discussed further above, has been established. This opportunity has been repeatedly taken in the context of the mathematical modeling of bone, in particular so for the determination of pore pressures in the intermolecular, intercrystalline, lacunar, and vascular pore spaces under various physiologically relevant loading scenarios [46,128–130]. The vascular and lacunar pore spaces host the biological cells involved in bone remodeling: osteoclasts, osteoblasts, and osteocytes, see Sec. 5 and Fig. 9 for more details.

When the interest goes beyond “simple” eigenstress or eigenstrain averaging of a two-phase composite with only one phase being eigenstressed, interesting scale transition solutions concerning eigenstrains and eigenstresses can be obtained from the extension of the classical Eshelby-Laws matrix-inhomogeneity problems to eigenstressed matrix-inhomogeneity problems [15]. The solutions to such problems are again based on Green's functions, now in combination with a homogeneous elastic medium and two types of eigenstresses: the classical polarization stress explained further above, and an additional, physically motivated eigenstress, such as a pore pressure or an eigenstress associated with plastic strains. Benveniste's micro-to-macroscale transitions can then be extended to eigenstressed multiphase media, as outlined by Pichler and Hellmich [131]: Each phase is represented by an inhomogeneity in an infinite matrix subjected to remote auxiliary strains; however, now both the inhomogeneity and the matrix exhibit eigenstresses. Insertion of corresponding phase-specific homogeneous strains into the strain average rule yields a relation between the remote auxiliary strains, the RVE-related macroscopic strains, and the eigenstresses in the inhomogeneity and in the matrix, respectively. In order to eventually relate the eigenstresses in the auxiliary matrix to the RVE-related macroscopic eigenstresses, additional use of Levin's theorem is made, finally yielding the so-called concentration-influence relations. The latter is the cornerstone of Dvorak's “transformation field analysis” introduced in the early 1990s [132–134]: The strains in each phase are not only related to the RVE-related overall macroscopic strains (by the already discussed strain concentration tensor), but also to the eigenstrains in all other phases and in the considered phase itself (by means of so-called fourth-order influence tensors). Homogenization of eigenstressed media was particularly helpful for explaining the strength of bone, arising from ductile sliding between hydrated crystals followed by brittle failure of molecular collagen [35]: Therefore, elementary plastic strains fulfilling the flow and consistency rules of classical plasticity [135] were introduced at the level of the hydroxyapatite crystals at Level 2B of Fig. 1, and thereafter upscaled up to the level of macroscopic bone material. More recent studies based on the representation of Level 2B of Fig. 1 have revealed the elastoplastic failure behavior of the cement lines surrounding secondary osteons in Haversian bone from the surrounding bone matrix [55].

3.5 Extensions Concerning the Large Strain Regime. Yet further extension of the use of Eshelby problems for scale transitions in complex materials concerns large deformations, the typical biological example being soft tissues. As compared to hard tissues, this challenge has only recently been tackled. First success approaches dealing with arterial and tendinous tissues [74,136] were mainly based on (i) re-formulation of the Eshelby problem

for velocity gradients (rather than linearized strains), allowing for the derivation of concentration relations between macroscopic strain rates on the one hand, and microscopic strain and spin rates, on the other hand; as well as on (ii) thermodynamically consistent hypoelastic material laws [137,138], linking objective (i.e., observer-independent) phase properties. Such Eshelby problem-based approaches may well help to overcome persisting difficulties in hierarchical soft tissue modeling. The latter include (i) the incomplete description of load-induced (micro-)fiber kinematics in the context of deformation gradient-based (hyperelastic) models, requiring rather complex, computationally expensive remedies [139,140]; and (ii) the similarly high computational expense of fiber network models [141–144], which, in addition, do not provide explicit access to the matrices found in between the fibers.

As a rule, the usefulness of all the aforementioned applications of scale transition techniques to biological and biomedical materials needs to be shown through careful and extensive experimental validation. This is the topic of the next section.

4 Experimental Validation—Different Methods at Different Scales

4.1 General Strategy. According to Popper’s famous reasoning on the logic of scientific discovery [145,146], a hypothesis which the human mind comes up with needs to survive as many statistically and physically different falsification tests as possible, in order to eventually reach, after extensive discussions and debates between the peers within a scientific community, the status of a reliable scientific theory. In this spirit, various multiscale micromechanics approaches, as described in Sec. 3, have been carefully validated by means of biomechanical, biophysical, and biochemical experiments [23,35,47,49,52,55,147]. Typically, such experiments concern

- (i) “universal”, i.e. tissue-invariant, mechanical properties of the elementary components making up any tissue belonging to a particular class of tissues (e.g., in the case of bone tissues: molecular collagen type I (making up around 90% of all organic matter found in bone [148]), hydroxyapatite, and water with non-collagenous organic, see Secs. 4.2–4.4 for details);
- (ii) tissue-specific mechanical properties at any hierarchical level above that of the elementary constituents, tested across the vertebrate animal kingdom, see Secs. 4.2 and 4.4 for details, and
- (iii) tissue-specific compositional information which can be converted into phase volume fractions, phase shapes, and phase interaction patterns at any hierarchical level above that of the elementary constituents, again tested across the vertebrate animal kingdom, see Sec. 4.5 for further details.

Based on these tests, the validation strategy is as follows:

- (i) the “universal” properties of the elementary components are associated with the phases which are not anymore resolved into RVEs themselves (i.e. in the case of bone illustrated in Fig. 1 to crosslinked molecular collagen, to hydroxyapatite, and to the intermolecular, intercrystalline, lacunar, and vascular pore spaces);
- (ii) the micromechanical model is fed with phase-specific volume fractions arising from biochemical and biophysical tests as detailed further below; and
- (iii) the respective model predictions in terms of the mechanical properties associated with the different RVEs are compared to corresponding experimental data on the very same mechanical properties.

This validation strategy has been particularly successful in the context of bone and mineralized tissues; and this concerns different types of mechanical properties, associated with elasticity [23,41,48,49,51,53,61,65,66,115,147], viscoelasticity [117],

poroelasticity [128–130], and elastoplasticity/strength [35,55,149]. We note in passing that scattering in material properties typically *decreases* upon elastic homogenization from smaller to larger scales [150]; and we continue with a more detailed account of the various experimental techniques that have provided data for the aforementioned model validation strategies. The term “universal” in the above paragraphs makes reference to the concept of architectural constraints governing the universal patterns which are omnipresent in the living world, classically discussed in the context of evolutionary biology [151,152]; later, this discussion has been extended toward a mathematical setting for hierarchical biomaterials mechanics [47].

4.2 Ultrasonic Pulse Transmission and Brillouin Light Scattering Measurements—Elastic Properties of Tissues and Their Elementary Components. Ultrasonic measurements refer to a very wide range of testing devices, including elastography which “aims at quantitatively image the Young’s E modulus, the physical parameter corresponding to the stiffness”, typically throughout larger portions of the organ [153].

Our present focus is different, and concerns the characterization of a particular material sample rather than a larger portion of an organ, and more precisely, the determination of several components of the elasticity tensor defining tissue properties at different length scales. In elastic media, the product of the squared pulse velocity with the sample’s mass density gives access to the components of the elasticity tensor [154]. However, ultrasonic tests may also give access to the elastic properties of media which are not behaving purely elastically. In more detail, for impulse frequencies associated with oscillation periods which are much shorter than the characteristic creep times of elasto-viscous materials, the wave velocity is linked to the instantaneous elastic properties of the material, even if the latter may show also inelastic deformations [154]. It is important to note that the actually tested RVE is determined through the wavelength, with the characteristic length of the RVE being five to ten times smaller than the wavelength [155], see Fig. 4. Ultrasonic tests have been very successfully employed for biological and biomedical material characterization, both at the fundamental level of the elementary constituents of a biological tissue class and at various levels of hierarchical organization. In the case of bone, ultrasonic tests at different frequencies give access to the majority of the RVEs depicted in Fig. 1 [23,47,147]: 10 MHz tests [70,156–158] refer to the extracellular bone material (Level 3 of Fig. 1); 2.25 MHz tests [159–161] refer to the extravascular bone matrix (Level 4 of Fig. 1), and 50 kHz tests [162–164] refer to the macroscopic (here trabecular) bone material (Level 5 of Fig. 1).

Ultrasonic tests have also provided access to the elastic properties of the aforementioned elementary components of bone: The bulk modulus of water amounts to 2.3 GPa [165]; and compared to this value, the shear modulus is negligibly small; tests on dense hydroxyapatite powder reveal an isotropic elastic Young’s modulus of 114 GPa and a Poisson’s ratio of 0.27 [166]. The elementary component “type I collagen” was elastically characterized by Cusack and Miller [167], by an interesting variant of ultrasound transmission concerning very high frequencies, called Brillouin light scattering. Namely, the speed of thermally excited elastic waves is measured in terms of the inelastic scattering of light which these waves emit. The employed 10 GHz signals refer to wavelengths of 300–400 nm, hence characterizing an RVE of some tens of nanometers characteristic length, i.e., to Level 1 in Fig. 1. In more detail, Cusack and Miller tested rat tail tendon, which, upon drying, collapses to a material consisting almost exclusively of type I collagen [168,169] and hence, represents “molecular collagen” phase of the RVE of Level 1 in Fig. 1 [47,49]. This reasoning was further refined [168] by considering xylene imbibition tests [170], showing that dried collagen still exhibits 12% intermolecular porosity in the sense of Level 1 of Fig. 1; and most interestingly, hydration-dependent wave velocity

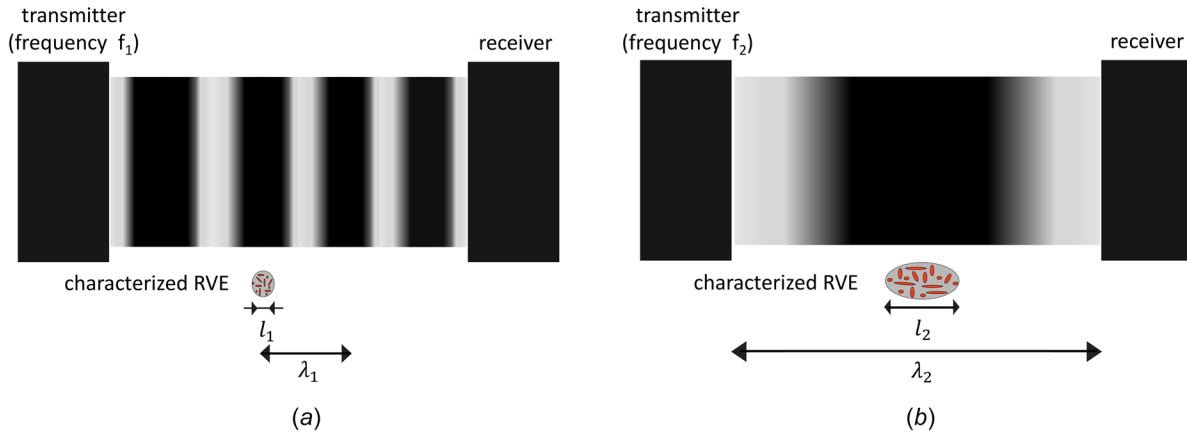


Fig. 4 Elasticity testing by means of ultrasonic pulse transmission: (a) higher frequency and (b) lower frequency pulse induce (a) shorter and (b) longer acoustic wavelengths, characterizing (a) smaller and (b) larger RVEs: RVE stiffness components are proportional to the square of the pulse velocity; figure adapted from [47], with permission from Elsevier

changes reported by Cusack and Lees [171] could indeed be traced back to composite material behavior in the sense of the RVE of Level 1 in Fig. 1. However, the issue might get trickier once a critical water-to-organic mass ratio of about 0.45 is exceeded: then, conformational changes of the molecular collagen itself are probable to lower its intrinsic elastic stiffness.

4.3 Persistence Length- and Bending Energy-Based Evaluation of Electron Micrographs—Elastic Properties of Long, Wound Bio-Macromolecules. Totally different from high-frequency elastic waves, the geometrical configurations of biomacromolecules, as observed under the electron microscope, may also give access to their elastic properties. The respective conceptual and theoretical foundations are as follows [172,173], see also Fig. 5: The investigated biomacromolecule is considered as a

long, wound thread approximated by a two-dimensional curve of arbitrary (differentiable) shape. Starting from a chosen origin, all the points on the curve are labeled by a contour length variable, and each of these points is assigned to the cosine of the angle between the tangent to the curve at the specific point, and the tangent to the curve at the origin. This process is repeated for many different origins and averaged over all the associated cosine-length relations: As a result, the average over the cosines of angles between any two tangents with a particular contour length between, decays exponentially when considered as function of the aforementioned (increasing) contour length; starting with one, and eventually tending to zero. The length characteristic quantifying this exponential decay is called persistence length. For small angles, the cosine can be expressed by means of the square of the angle, with the latter becoming a function of the contour length and the persistence length, see Fig. 5. The key to relating this

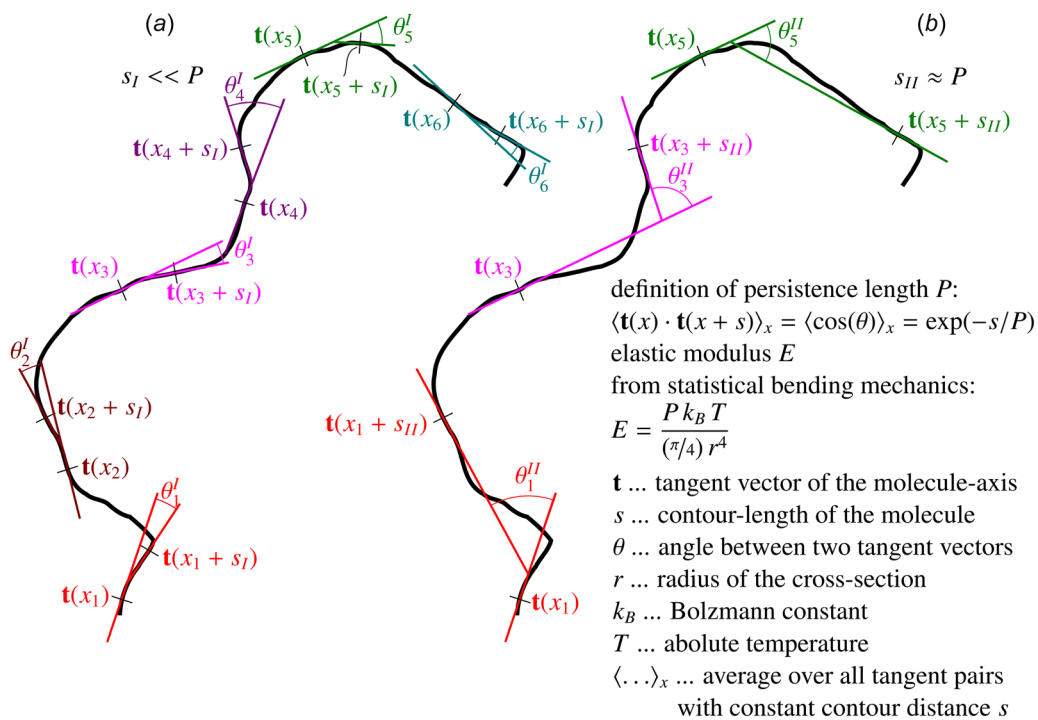


Fig. 5 Determination of persistence length P , and associated elastic modulus E , from electron micrograph of long collagen molecules: (a) tangents to molecular curve hardly vary over distances s_I , which are short when compared to the persistence length and (b) show large variability over long distances s_{II}

statistical distribution of “bending angles” between tangents, to mechanical properties lies in the consideration of different bending energy states, each of which can also be expressed in terms of a bending angle and a contour length. Moreover, the bending energy states follow a Boltzmann distribution governed by the absolute temperature. Equating the Boltzmann distribution-related average of the square of the bending angles, to the corresponding average obtained from the geometrical evaluation of the biomacromolecule’s shape, finally provides the bending stiffness (also referred to as flexural rigidity) as a function of the persistence length, the Boltzmann constant and the absolute temperature. When considering, in addition, the biomacromolecule to have a circular cross section, standard beam theory can be used for relating the bending stiffness to the Young’s (elastic) modulus of the “material” making up the biomacromolecule. In the case of collagen type I molecule with side chains in a biologically relevant conformation [174–177] a cross-sectional diameter of 1.4 nm, together with a persistence length of 57 nm, results in an elastic modulus of approximately 3 GPa.

4.4 Quasi-Static Mechanical Tests: (Visco-)Elastic and Strength Properties. The epitome of biomechanical testing is uni-axial quasi-static experiments, where a cuboidal or cylindrical sample is subjected uni-axially to tension or to compression forces, see Fig. 6. Care needs to be taken in order to realize, as far as possible, homogeneous uni-axial mechanical stress states, with a magnitude amounting to that of the applied force divided by the area over which the force is transferred onto the material sample. These mechanical stresses are related to length changes of the sample. The latter may be recorded by very elaborate techniques, such as wide angle X-ray scattering in order to detect length changes at the level line elements which are as small as 0.29 nm [178]. Corresponding tension tests on bovine achilles tendon confirmed the 3 GPa elastic modulus of collagen, as referred to above in Sec. 4.3. Collagen is known to behave, in a fairly good approximation, elastically upon loading, with an abrupt transition from elastic deformations to brittle fracture, as can be inferred from tensile tests on collagen fibers [179]. However, this is not the case any more with more complex composite-type materials such as bone, where elasto-plastic behavior is encountered already at low loading levels [35,55,180].

In order to retrieve elastic properties from such tests, the thermodynamic nature of elasticity needs to be carefully considered [2,3,9,181]: Elastic energy is that portion of the internal energy stored in the material, which can be back-transformed into

efficient mechanical work. This transformation happens once a sample is unloaded. Hence, slopes in the loading regime of mechanical tests encompass both (visco-)elastic and plastic portions, and only the unloading regimes guarantee the absence of plastic deformations. Accordingly, moduli derived from the loading portions of stress–strain curves qualify as “(visco-)elasto-plastic”, and only the unloading branches of stress–strain curves are associated with (visco-)elasticity only [182–185]. In this context, we also note that the mineral and water contents are key drivers of bone viscoelasticity: This underlines the importance of the hydrated extrafibrillar polycrystal for the dissipative mechanical behavior of bone [117,182,186,187].

When it comes to strength, there is virtually no alternative to mechanical tests. However, in the context of strength, the load is not lowered so as to get access to (visco-)elastic properties, but it is increased up to mechanical failure of the sample. Accordingly, the strength properties of the elementary components of bone (collagen and hydroxyapatite) were inferred from uni-axial mechanical tests where rat tail tendons [179] and samples of densely compacted hydroxyapatite powder [189,190] have been loaded up to failure. The strength of the extracellular bone material can be gained from micropillar testing [188,191,192], the strength of polycrystalline material making up the cement lines around osteons can be accessed through osteon push-out tests [193], and the strength of macroscopic bone materials has been amply tested over the last five decades (at least). In this context, it is advisable to prefer tests where homogeneous stress states prevail in the sample, such as uni-axial tension tests and uni-axial compression tests [194–211]. For example, bending tests deliver much less reliable results as major hypotheses concerning material and structural behavior need to be made. Normally, such hypotheses have been readily borrowed from engineering steel construction—however, as actually evident from abundant mechanical and chemical features, bone is obviously not steel.

4.5 Physico-Chemical Tests—Textural and Compositional Properties. In this context, demineralization, decollagenization, and/or dehydration tests, in combination with weighing tests, Archimedes’ principle, inductively coupled optical emission spectroscopy (ICP-OES), and microscopic investigations [69,212–218] are the key experimental access to the chemical composition of bone ultrastructure. Surprisingly, across many different bone tissues of differently aged mammalian and avian species, there emerges a clear bilinear relationship between the apparent mass densities of mineral and organic matter (i.e., of the

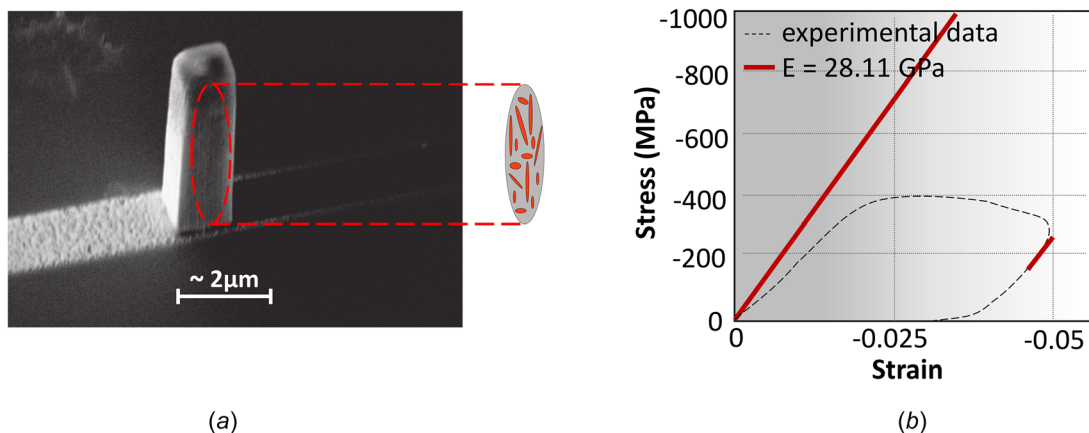
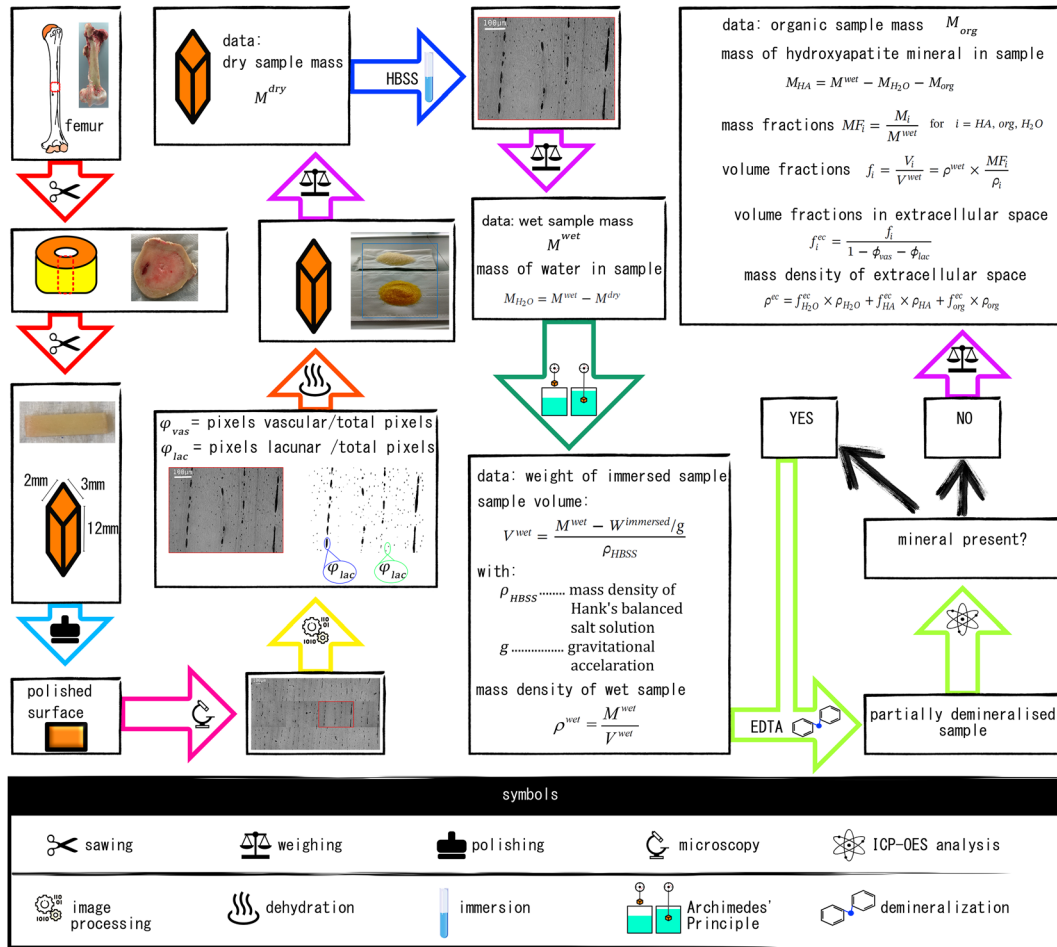


Fig. 6 Quasi-static mechanical testing: (a) single micrometer-sized cuboid sample of bovine femoral bone; prepared, by means of focused ion beam milling, for uni-axial testing through a flat punch installed in a nano-indenter setting [188], (b) corresponding stress–strain curve characterizing micrometer-sized RVE in loading and unloading mode [188]; the latter gives access to the elastic Young’s modulus. The image of the bovine femoral bone sample shown in (a) was extracted from Ref. [188], the corresponding stress–strain curve shown in (b) was adapted from Ref. [188], with permission from Elsevier.

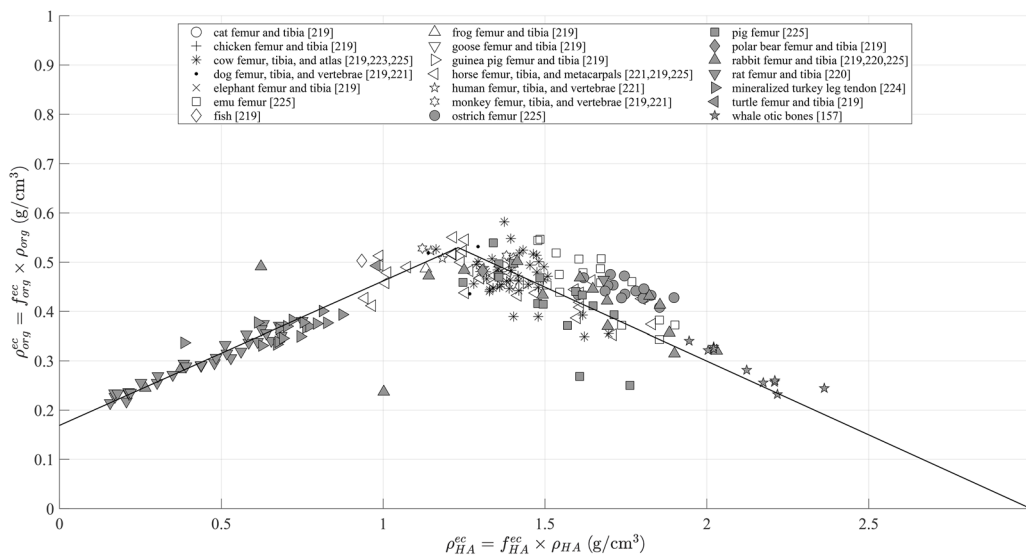
masses of mineral and organic matter divided by the volume of extracellular matrix within which they reside), see Fig. 7 [157,219–225].

When additionally considering X-ray and neutron diffraction tests giving access to the distance between collagen molecules,

several “universal” rules concerning the composition and microstructure of mineralized collagenous tissues (such as bone) can be derived: (i) upon hydration, the extrafibrillar space grows proportionally to the fibrillar swelling in nonmineralized collagenous tissues [168]; (ii) within the bone ultrastructure, the average



(a)



(b)

Fig. 7 Sequence of dehydration, demineralization, and weighing tests: (a) scheme and (b) resulting bilinear organic-to-mineral relationship

extrafibrillar, and the average extracollagenous mineral concentration are the same [226]; (iii) the mineral and collagen volume fractions within the extracellular bone matrix are linearly related to each other [227]; and (iv) tissue shrinkage upon mineralization can be explained from precipitation of mineral from a liquid solution under closed thermodynamic conditions [228]. These rules yield the tissue-specific volume fractions within the RVEs of Levels 1 to 3 in Figs. 1 and 3; while the pore volume fractions at the higher levels are accessible from light microscopy [225] or computed tomography (CT) [229]. On top of that, the RVE representation of the bone ultrastructure has independently been confirmed by an electrodynamic model based on Maxwell's equations [230].

4.6 Whole Bone Tests—Model Validation at the Organ Scale, in Terms of Safety Levels and Ultimate Structural Strength. Experimentally validated material properties retrieved from hierarchical biomechanics models for level 5 of Fig. 1 can also be used for feeding structural mechanics models of organs, such as an FE model of a lumbar vertebra as seen in Fig. 8. Such models are typically derived from CT [231–233]. Thereby, the CT data gives access to (i) the topology of the organ and (ii), via the average rule for X-ray attenuation coefficients [234,235], to heterogeneous fields of vascular porosities throughout the organ. When additionally accounting for the invariance over space and time of the organ-specific chemical composition of the bone ultrastructure when averaged over millimeter-sized domains [225,236–239], and of the correspondingly invariant volume fractions inside the RVEs of the ultrastructure level and below, the aforementioned homogenization schemes provide inhomogeneous mechanical property distributions throughout the FE models. Eventually, this allows for the estimation of patient- and activity-specific safety factors of a load-bearing organ; elucidating that mild physiological loading of a lumbar vertebra is associated with a safety factor of around five [231], see Fig. 8. This value is fully consistent with the ultimate forces obtained from mechanical tests on whole vertebrae [240–243] as well as with loadings encountered in the context of extreme sports activities [244]. Similar types of structural modeling have been realized for various other systems, including human and murine femora [233,245,246], human mandibles [232,247], or different tissue engineering constructs [88,96,122,123,248].

5 Perspectives on Hierarchy-Related Aspects in Mechanobiology, Single Cell Mechanics, and Biomacromolecules

As is evident from the preceding sections, hierarchical biomechanics has most maturely evolved in the case of bone tissue, with

first interesting approaches appearing for other tissues as well. All these results concern mechanical properties, and how they are related to tissue composition and organization. However, hierarchical modeling may still enter the picture in a yet broader scope, namely, when studying the interplay between mechanics and biology, either at the hierarchies found in tissues or within individual biological cells themselves, down to the level of individual biomacromolecules such as DNA. This broadened vision of “hierarchical biomechanics” is the scope of the present subsection.

5.1 Toward Hierarchical Mechanobiology. When dealing with biological tissues, it is well known that the mechanical loading they are subjected to may have a substantial influence on the biological processes responsible for maintaining their integrities, or even for their sizes and shapes [249–253]. In more detail, mechanical loading is usually applied macroscopically, and is somehow transferred to the scale of cellular processes or even below, where corresponding mechanical stimuli influence the occurrence and behavior of biological factors. Hence, multiscale mechanobiology involves, *per se*, multiscale (poro-)mechanics, on the one hand, and multiscale systems biology, on the other hand. Multiscale (poro-)mechanics has already been dealt with in the previous sections, and it has been successfully applied to bone tissue, in order to estimate mechanical stimuli occurring on the cell scale in response to macroscopically applied mechanical loading; see, e.g., [46,254–258]. These examples are based on or inspired by continuum micromechanics as underlying concept. As an alternative, numerical homogenization approaches similar to those described in Sec. 3.1 have been used for studying bone regeneration guided by tissue engineering scaffolds [85–87,259,260]. A rare, quite mature example of hierarchical mechanobiology, documented in Ref. [255], is illustrated in Fig. 9: The macroscopic (oscillating) loads applied to a bony organ, such as a human femur (see Fig. 9(a)), are first converted into local stresses associated with macroscopic RVEs, one of which is shown in Fig. 9(b). This RVE coincides with that of Level 5 in Fig. 1. The aforementioned stresses are then down-scaled to (oscillating) pore pressures in the vascular pores, where they affect the biochemical activities of two types of biological cells: osteoblasts and osteoclasts, see Fig. 9(d). Interestingly, physiological load levels translate into vascular pore pressures of the order of several tens of kilopascals [46]: This is the magnitude to which a large set of biological cells are reacting [261–277]. Further downscaling from the macroscopic RVEs of Fig. 9(b), to the level of lacunar pores (see Fig. 9(c)), delivers pore pressures of similar magnitude, stimulating osteocytes, as seen in Fig. 9(e). In more detail, the increase of lacunar and vascular pore pressures

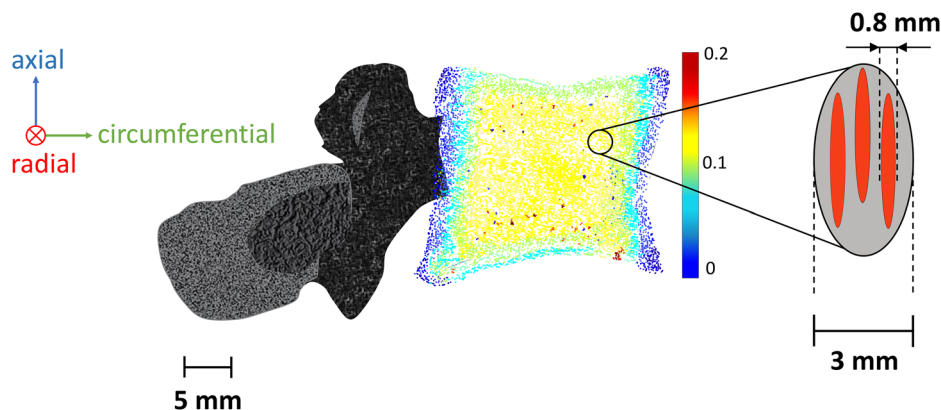
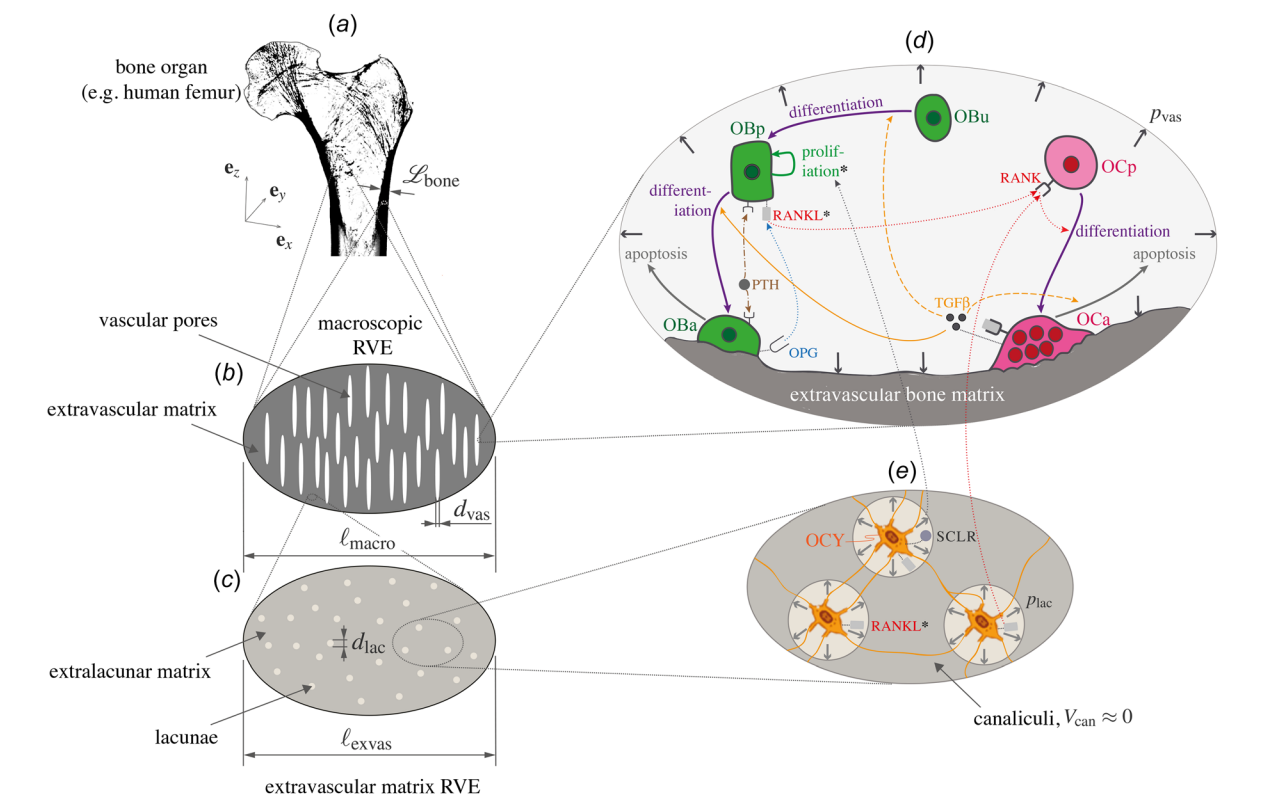


Fig. 8 Micromechanics-informed safety assessment of human lumbar vertebra under mild physiological loading, after [231]: FE model (a) is fed with local material properties retrieved from (b) RVE of level 5 according to Fig. 1; color represents loading degree with respect to ultimate load (100% relates to elastoplastic failure)



Abbreviations:
 OBa ... Active osteoblasts
 OBp ... Osteoblast precursors
 OBU ... Uncommitted osteoblast progenitors
 OCa ... Active osteoclasts
 OCp ... Osteoclast precursors
 OCY ... Osteocytes
 OPG ... Osteoprotegerin
 PTH ... Parathyroid hormone
 RANK ... Receptor of activator nuclear factor κB
 RANKL ... RANK ligand
 RVE ... Representative volume element
 SCLR ... Sclerostin
 TGFβ ... Transforming growth factor beta

Symbols:
 d_{lac} ... Characteristic length of lacunar pores
 d_{vas} ... Characteristic length of vascular pores
 e_i ... base unit vectors, $i = x, y, z$
 L_{bone} ... Characteristic length of bone organs
 l_{macro} ... Characteristic length of RVE of macroscopic bone tissue
 l_{exvas} ... Characteristic length of RVE of extravascular bone matrix
 p_{lac} ... Hydrostatic pressure in lacunar pores
 p_{vas} ... Hydrostatic pressure in vascular pores
 V_{can} ... Volume of canaliculi pores

Regulatory pathways:
→ Upregulation of OCp differentiation
→ Upregulation of OBU differentiation and of OCa apoptosis
→ Downregulation of OBp differentiation
→ Upregulation of RANKL production and downregulation of OPG production
→ Upregulation of OBp proliferation
 * Regulatory effect through hydrostatic pressures (downregulation of RANKL production and upregulation of OBp proliferation)

Fig. 9 The multiscale model proposed by Pastrama et al. [255] couples multiscale poromicromechanics of bone, providing the oscillatory hydrostatic pressure in the pore spaces hosting the bone cells (osteocytes, osteoblasts, osteoclasts), with a multiscale bone cells population model for bone remodeling, with the micromechanically derived pore-scale pressures as regulatory factors; figure adapted from Ref. [255], with permission from Elsevier

stimulates the proliferation of active osteoblasts. The latter builds up new extravascular bone matrix. At the same time, increasing lacunar and vascular pore pressures suppress the production of RANKL, i.e., of the key factor activating osteoclasts, the cells which dissolve extracellular bone matrix.

It is interesting to note that similarly large pressures occur in the extrafibrillar matrices of soft tissues, as has been quantified by the hierarchical tendon model of Morin et al. [136], also referred to in Sec. 3.5. This holds the promise for wide research opportunities unifying not only hard and soft biomechanics, but also hard and soft tissue mechanobiology.

Biological cells may not only populate pores with extracellular matrices making up tissues (the latter may be categorized as porous solids with largely varying stiffnesses), but they may also govern the behavior of complex fluids such as blood. The latter is made up of red blood cells, white blood cells, platelets, and plasma. From the viewpoint of “fluid micromechanics”, these four constituents would appear as “phases” making up a “fluid material system”. However, the nature of the dynamics of blood (standardly referred to as hemodynamics) rendered particle-based

methods [278], rather than semi-analytical solid mechanics methods, as particularly appropriate. Accordingly, biological entities such as cells or platelets are modeled as discrete particles. Moving from the blood itself back to the vessels in which it is contained, particle mechanics has also been beneficial in the context of atherosclerosis, where low-density lipoprotein (LDL) molecules enter into the intima, either through mediation of vesicles taking up LDL or through apoptosis-induced leaky junctions in the endothelium [279,280]. In this context, the so-called discrete particle dynamics (DPD) method turned out as particularly effective when it comes to simulating hydrodynamics of simple and complex liquids on a mesoscopic scale [281]. Details on the mathematical implementation of the DPD approach can be found, e.g., in Ref. [278,282–285], see also Fig. 10. A particularly illustrative example concerns the modeling of thrombosis as the interaction between activated platelets, forming aggregations among themselves and with the adjacent endothelial cells [283], see Fig. 11. Of similar interest is the DPD-based prediction of shear fluid stress-dependent initiation of atherosclerosis by means of binding LDL to the blood vessel walls [279].

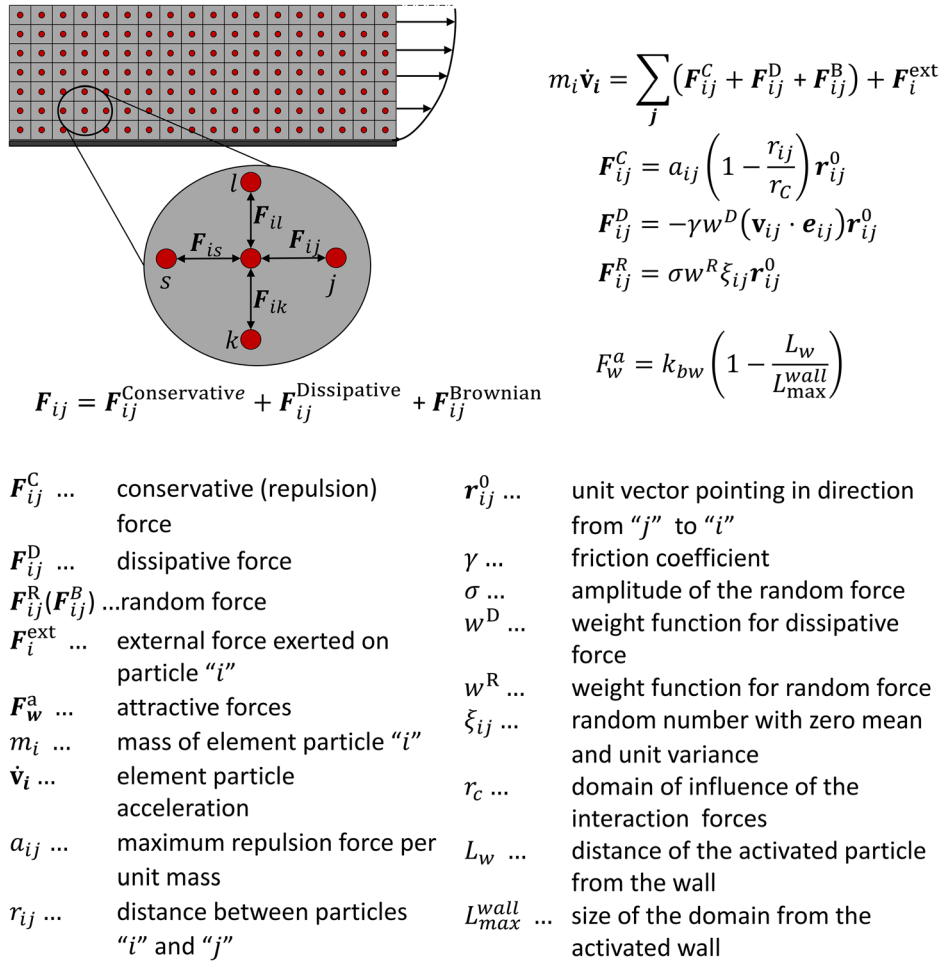


Fig. 10 Illustration of the fundamental principle of discrete particle dynamics approaches, including a brief sketch of the related mathematical framework, involving the forces acting onto the considered particles; drawing adapted from Ref. [283]

5.2 Hierarchies in the Mechanics of Single Cells and Bio-Macromolecules. We finally turn toward single biological cells and their internal structure: Traditional visco-elastic continuum models have been widely used to quantify cell mechanical properties [286]. Such models are convenient to help parameterize the results of mechanical measurements from techniques such as

atomic force microscopy (AFM), micropipette aspiration, microrheology, and parallel plate compression [287]. They offer a straightforward and minimal way to interpret differences between experimental conditions and summarize the results of mechanical measurements. When restricted to the timescale and spatial resolution of a specific measurement, these relatively simple

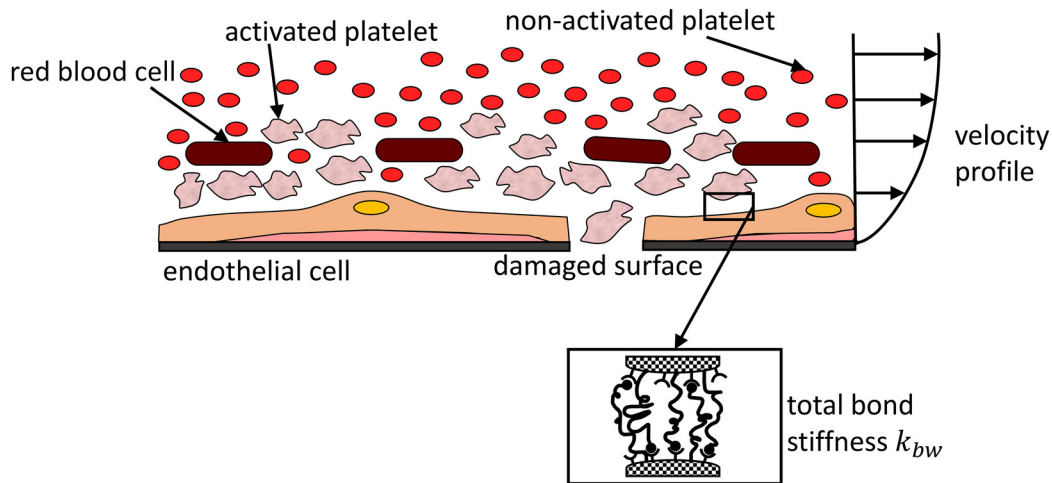


Fig. 11 Platelet aggregation and adhesion leading to thrombosis; the drawing follows Ref. [283]

mechanical models are in strikingly good agreement with observed mechanical behavior. For example, the force-indentation response obtained from an AFM measurement typically corresponds well to Hertz's theory for elastic bodies [288]. Under this framework, many model implementations have been introduced to analyze AFM experiments using visco-elastic theory, such as adaptations of Hertz theory for the specific contact geometry [289], models that consider the viscous response of the cell or the distinct mechanical properties of the actin cortex [290–292], and FEM analysis to represent the specific geometry of the cell and the position on the nucleus [293].

However, when generalizing mechanical properties across spatial and temporal scales, visco-elastic or poro-elastic constitutive models invariably break down. Instead, living cells appear like glassy materials that exhibit power law rheology when probed across time scales [294–296]. This property has been attributed to the cells active material properties [297]. At the microscopic scale, the mechanical behavior of a cell is governed by the cytoskeleton, a dynamic reorganizing polymer network that forms mechanically relevant structures at a broad spectrum of characteristic length scales, giving rise to self-similarity and fractals [298]. Furthermore, the cytoskeleton exhibits biphasic rheology, with frequent solid-to-fluid dynamics and even self-organized criticality in active structures such as the lamellipodium [299,300].

To date, the aforementioned properties have complicated homogenization attempts to model the mechanical behavior of intracellular material [301]. Indeed, the absence of a clearly defined microscopic (small) length scale prevents the straightforward formulation of “representative volume elements” in the pursuit of macroscopic constitutive equations. Successful attempts to model the mechanical properties of intracellular material at a cellular scale include coarse-grained representations of acto-myosin polymer networks and continuum models based on hydrodynamic theory of active fluids.

Coarse-grained molecular dynamics models of active polymers aim to provide a computationally minimal representation of the network structure formed by the cytoskeleton [302,303]. Typically, they include, as discrete elements, the filaments, and cross-linkers of acto-myosin or microtubule networks. Contrary to full-atomistic resolved molecular dynamics, they do not include atomic interactions, but instead are based on coarse-grained approximations of thermal forces, internal mechanics, and

interaction properties [304]. For example, the mechanical properties of polymers are commonly represented using worm-like chain models, whereas the asymmetry in attachment of myosin motors to actin filaments is modeled using a “ratchet” potential [305,306]. Various computational implementations of these discrete coarse-grained elements exist, such as bead-spring models, rod models, and FE representations of fibers [307]. As a whole, this family of models has been very successful in unraveling the mechanics of specific relevant cytoskeletal structures, such as polymerization in the lamellipodium, the attachment membrane or adhesion complexes, and the formation of stress fibers [308–310]. Moreover, they are particularly useful in studying artificial cytoskeletal structures, such as reconstituted acto-myosin networks, of which the well-known composition and chemical conditions greatly facilitate mechanistic model formulation [311]. Vice versa, such artificial structures provide convenient test beds to calibrate and validate simulations of coarse-grained polymer assemblies. Alternatively, these systems can be experimentally studied at submicroscopic scales, using techniques such as active and passive microrheology [312]. Nonetheless, the applicability of this family of models in the context of a biological cell is limited, not only due to computational limitations, restricting the spatio-temporal scale of the domain, but also due to the inability to exhaustively represent the complex environment in intracellular material.

At the other end, hydrodynamic models of active fluids (or active “gels”) are constitutive continuum models that represent a relevant subset of behaviors of intracellular material [313,314]. In poroviscous theory, pioneered in the context of cells by Dembo and coworkers, the intracellular material is modeled as two coupled interpenetrating fluids, the cytosol and a gel-like cytoskeletal network [315]. By addition of signaling-coupled reaction terms for network assembly and disassembly, these models can simulate various cell dynamical processes. Active nematic theory combines the hydrodynamic equations of an active—typically, contractile—fluid with a polar or apolar director field. In doing so, it is able to capture the intrinsic anisotropy of the underlying network and the spontaneous flow as a result of contractile forces generated by myosin activity [316]. Since they are essentially fluid models, these models are generally unable to describe the elastic mechanical response that would be measured in a typical AFM measurement [317]. However, they provide a very useful

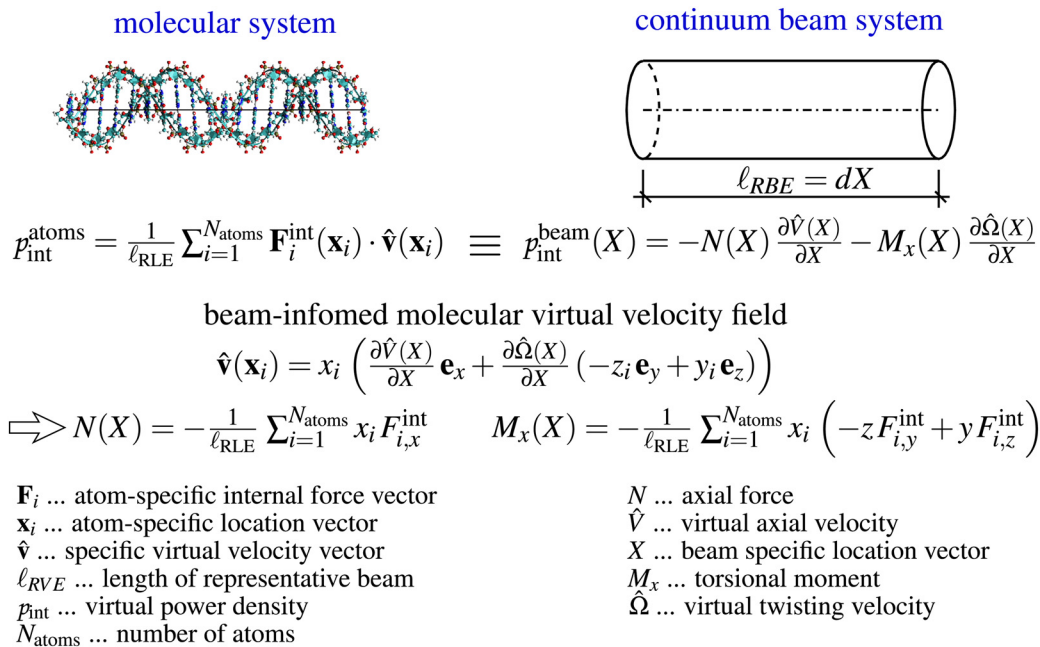


Fig. 12 Atoms-to-beam homogenization of DNA molecules [325]

tool to help understand the intracellular flows that allow the cell to reorganize itself over longer timescales. For example, simulations using these models have been instrumental in explaining the role of the dynamical organization of actin filaments in furrow formation during development [318,319]. Furthermore, the emergence of spontaneous cell division and cell motility has been observed in models that combine active nematics with poroviscous theory [320].

To address the shortcomings of these limiting conceptual frameworks, various hybrid modeling approaches have been proposed that combine discrete coarse-grained networks with hydrodynamic continuum equations or simplified phenomenological models [321]. These attempts have yielded important insights into specific cell mechanical processes such as bleb initiation, protrusion formation, or cell-matrix interaction [322]. Operating at the cellular scale, these models are used to study mechanisms of active force generation and mechanotransduction. As such, they are suitable for the interpretation of traction force microscopy measurements, in which active forces are quantified by measuring the deformation of a well-characterized substrate. For example, a hybrid model that combines discrete tensional cables in a continuum contractile material was able to relate forces exerted by the cell on the substrate to the generated tension in actin stress fibers [323]. However, these hybrid modeling frameworks are generally limited to specific phenomena, with an associated reduction in spatio-temporal scales. As such, the formulation of a general modeling methodology for describing cell mechanical behavior, based on measurable microscopic parameters and amenable to homogenization for multiscale models, remains a major scientific challenge [317].

A perspective toward overcoming this major challenge recently emerged from a very classical concept in continuum mechanics: the principle of virtual power in its most modern format put forward by Germain [324]: This principle is a natural merger of the laws of equilibrium (or motion in case of inertia forces) with the kinematical characteristics of the investigated mechanical system. Accordingly, it states that the virtual power of internal, external, and inertial forces on arbitrary admissible virtual velocity fields defining the kinematical nature of the considered mechanical system, need always to be zero. Given the current atomistic-to-continuum homogenization challenge, identification of the virtual power performed by equilibrated molecular dynamics-derived atomistic forces in different configurations of the investigated system, on virtual velocity fields characterizing macromolecular kinematics in terms of beam-theory-type continuum notions (stretching, twisting, bending) opened a new avenue to study coupled deformation modes in DNA [325], see Fig. 12: Stretching and twisting of these long double-helical macromolecules are, as a rule, coupled, and the type of coupling depends on the deformational state. This may hold the promise to come up with a new type of structural mechanics which is complex and at the same time stable enough, so as to effectively build up a new, mechanics-driven, addition to the current state of the art in genetics and cell biology. These most probably worthwhile endeavors have been recently coined as “mechanobiome” research [326]. It holds the promise to integrate the vast “computational wisdom” accumulated for DNA and other biomacromolecules [327–329] into (micro)structural mechanics terms, allowing for linking this “condensed wisdom” to the wide field of hierarchical biomechanics. More precisely, any characteristics emerging through homogenization over the atoms making up the biomolecules, and over the latter seen as structural members with appropriately defined mechanical properties, may provide radically new knowledge for at least two challenging open fields in bio-engineering and the life sciences: (i) deeper, and more quantitative, understanding of mechanical stimulation properties of overall biological cells, which could then enter hierarchical models as the one seen in Fig. 9; and (ii) more comprehensive insight into the mechanical competence of extracellular matrices under extreme, i.e., also pathological, conditions, as additional input for hierarchical models as the one shown in Fig. 1.

6 Conclusions

A set of several scale-specific representative volume elements, nested among each other and each equipped with stress and strain average rules, as well as with scale transition rules for elastic as well as inelastic strains, allows for the prediction of mechanical properties from composition and organization of biological tissues. This has been shown in greatest detail in the case of bone, by combining analytical or computational homogenization schemes with the data obtained from a variety of biochemical, biophysical, and biomechanical experiments. Recent research results suggest a similarly, high potential for the soft tissue regime, and hierarchical modeling approaches seem particularly promising in the fields of mechanobiology (where biological cells are “inserted” into the tissues’ pore spaces) and cell/biomacromolecule mechanics.

Acknowledgment

The authors gratefully acknowledge the financial support granted by the European Commission in the framework of the project Increasing scientific, technological, and innovation capacity of Serbia as a widening country in the domain of multiscale modelling and medical informatics in biomedical engineering (SGABU), Grant Agreement No. 952603.

Funding Data

- European Commission (Funder ID: 10.13039/501100000780).

Nomenclature

- AFM = atomic force microscopy
- CT = computed tomography
- DPD = discrete particle dynamics
- FE = finite element
- FFT = fast Fourier transform
- ICP-OES = inductively coupled optical emission spectroscopy
- LDL = low-density lipoprotein
- RANKL = receptor of activator nuclear factor κ B ligand
- RVE = representative volume element

References

- [1] Alber, M., Buganza Tepole, A., Cannon, W., De, S., Dura-Bernal, S., Garikipati, K., Karniadakis, G., Lytton, W., Perdikaris, P., Petzold, L., and Kuhl, E., 2019, “Integrating Machine Learning and Multiscale Modeling – Perspectives, Challenges, and Opportunities in the Biological, Biomedical, and Behavioral Sciences,” *NPJ Digital Med.*, **2**(1), pp. 1–15.
- [2] Rajagopal, K. R., 2007, “The Elasticity of Elasticity,” *Z. Für Angewandte Mathematik Und Phys.*, **58**(2), pp. 309–317.
- [3] Coleman, B. D., and Noll, W., 1961, “Foundations of Linear Viscoelasticity,” *Rev. Mod. Phys.*, **33**(2), pp. 239–249.
- [4] Boltzmann, L., 1874, “Zur Theorie Der Elastischen Nachwirkung [Concerning the Theory of the Elastic Aftereffect],” *Sitzungsberichte Der Mathematisch-Naturwissenschaftlichen Classe Der Kaiserlichen Akademie Der Wissenschaften*, **70**(2), pp. 275–306 [In German].
- [5] Xiao, H., Bruhns, O. T., and Meyers, A., 2006, “Elastoplasticity Beyond Small Deformations,” *Acta Mech.*, **182**(1–2), pp. 31–111.
- [6] Melan, E., 1938, “Zur Plastizität Des Räumlichen Kontinuums [Concerning Plasticity of the Spatial Continuum],” *Ingenieur-Archiv*, **9**(2), pp. 116–126 [In German].
- [7] Weiner, S., and Wagner, H. D., 1998, “The Material Bone: Structure-Mechanical Function Relations,” *Annu. Rev. Mater. Sci.*, **28**(1), pp. 271–298.
- [8] Lakes, R., 1993, “Materials With Structural Hierarchy,” *Nature*, **361**(6412), pp. 511–515.
- [9] Coussy, O., 2004, *Poromechanics*, Wiley, Chichester, UK.
- [10] Biot, M., 1941, “General Theory of Three-Dimensional Consolidation,” *J. Appl. Phys.*, **12**(2), pp. 155–164.
- [11] Thompson, M., and Willis, J., 1991, “A Reformation of the Equations of Anisotropic Poroelasticity,” *ASME J. Appl. Mech.*, **58**(3), pp. 612–616.
- [12] Gassmann, F., 1951, “Über Die Elastizität Poröser Medien [on the Elasticity of Porous Media],” *Vierteljahrsschrift Der Naturforschenden Gesellschaft Zürich*, **96**, pp. 1–23 [In German].
- [13] Zhang, D., Weinbaum, S., and Cowin, S., 1998, “On the Calculation of Bone Pore Water Pressure Due to Mechanical Loading,” *Int. J. Solids Struct.*, **35**(34–35), pp. 4981–4997.

- [14] Cowin, S., 1999, "Bone Poroelasticity," *J. Biomech.*, **32**(3), pp. 217–238.
- [15] Zaoui, A., 2002, "Continuum Micromechanics: Survey," *J. Eng. Mech. (ASCE)*, **128**(8), pp. 808–816.
- [16] Hill, R., 1963, "Elastic Properties of Reinforced Solids: Some Theoretical Principles," *J. Mech. Phys. Solids*, **11**(5), pp. 357–372.
- [17] Hashin, Z., 1983, "Analysis of Composite Materials – A Survey," *ASME J. Appl. Mech.*, **50**(3), pp. 481–505.
- [18] Drugan, W., and Willis, J., 1996, "A Micromechanics-Based Nonlocal Constitutive Equation and Estimates of Representative Volume Element Size for Elastic Composites," *J. Mech. Phys. Solids*, **44**(4), pp. 497–524.
- [19] Gusev, A. A., 1997, "Representative Volume Element Size for Elastic Composites: A Numerical Study," *J. Mech. Phys. Solids*, **45**(9), pp. 1449–1459.
- [20] Grimal, Q., Raum, K., Gerisch, A., and Laugier, P., 2011, "A Determination of the Minimum Sizes of Representative Volume Elements for the Predictions of Cortical Bone Elastic Properties," *Biomech. Model. Mechanobiol.*, **10**(6), pp. 925–937.
- [21] Dormieux, L., Molinari, A., and Kondo, D., 2002, "Micromechanical Approach to the Behavior of Poroelastic Materials," *J. Mech. Phys. Solids*, **50**(10), pp. 2203–2231.
- [22] Hollister, S. J., and Kikuchi, N., 1994, "Homogenization Theory and Digital Imaging: A Basis for Studying the Mechanics and Design Principles of Bone Tissue," *Biotechnol. Bioeng.*, **43**(7), pp. 586–596.
- [23] Hellmich, C., Ulm, F.-J., and Dormieux, L., 2004, "Can the Diverse Elastic Properties of Trabecular and Cortical Bone Be Attributed to Only a Few Tissue-Independent Phase Properties and Their Interactions?," *Biomech. Model. Mechanobiol.*, **2**(4), pp. 219–238.
- [24] Colloca, M., Blanchard, R., Hellmich, C., Ito, K., and van Rietbergen, B., 2014, "A Multiscale Analytical Approach for Bone Remodeling Simulations: Linking Scales From Collagen to Trabeculae," *Bone*, **64**, pp. 303–313.
- [25] Goda, I., Assidi, M., and Ganghoffer, J. F., 2014, "A 3D Elastic Micropolar Model of Vertebral Trabecular Bone From Lattice Homogenization of the Bone Microstructure," *Biomech. Model. Mechanobiol.*, **13**(1), pp. 53–83.
- [26] Abdalrahman, T., Scheiner, S., and Hellmich, C., 2015, "Is Trabecular Bone Permeability Governed by Molecular Ordering-Induced Fluid Viscosity Gain? Arguments From Re-Evaluation of Experimental Data in the Framework of Homogenization Theory," *J. Theor. Biol.*, **365**, pp. 433–444.
- [27] Basaruddin, K. S., Takano, N., Akiyama, H., and Nakano, T., 2013, "Uncertainty Modeling in the Prediction of Effective Mechanical Properties Using Stochastic Homogenization Method With Application to Porous Trabecular Bone," *Mater. Trans.*, **54**(8), pp. 1250–1256.
- [28] Panyasantisuk, J., Pahr, D. H., Gross, T., and Zysset, P. K., 2015, "Comparison of Mixed and Kinematic Uniform Boundary Conditions in Homogenized Elasticity of Femoral Trabecular Bone Using Microfinite Element Analyses," *ASME J. Biomechanical Eng.*, **137**(1), p. 011002.
- [29] Pahr, D., and Zysset, P., 2008, "Influence of Boundary Conditions on Computed Apparent Elastic Properties of Cancellous Bone," *Biomech. Model. Mechanobiol.*, **7**(6), pp. 463–476.
- [30] Hammond, M. A., Wallace, J. M., Allen, M. R., and Siegmund, T., 2018, "Incorporating Tissue Anisotropy and Heterogeneity in Finite Element Models of Trabecular Bone Altered Predicted Local Stress Distributions," *Biomech. Model. Mechanobiol.*, **17**(2), pp. 605–614.
- [31] Hogan, H. A., 1992, "Micromechanics Modeling of Haversian Cortical Bone Properties," *J. Biomech.*, **25**(5), pp. 549–556.
- [32] Grimal, Q., Rus, G., Parnell, W. J., and Laugier, P., 2011, "A Two-Parameter Model of the Effective Elastic Tensor for Cortical Bone," *J. Biomech.*, **44**(8), pp. 1621–1625.
- [33] Dong, X. N., and Guo, X. E., 2006, "Prediction of Cortical Bone Elastic Constants by a Two-Level Micromechanical Model Using a Generalized Self-Consistent Method," *ASME J. Biomech. Eng.*, **128**(3), pp. 309–316.
- [34] Hamed, E., Lee, Y. H., and Jasiuk, I., 2010, "Multiscale Modeling of Elastic Properties of Cortical Bone," *Acta Mech.*, **213**(1–2), pp. 131–154.
- [35] Fritsch, A., Hellmich, C., and Dormieux, L., 2009, "Ductile Sliding Between Mineral Crystals Followed by Rupture of Collagen Crosslinks: Experimentally Supported Micromechanical Explanation of Bone Strength," *J. Theor. Biol.*, **260**(2), pp. 230–252.
- [36] Parnell, W. J., Vu, M. B., Grimal, Q., and Naili, S., 2012, "Analytical Methods to Determine the Effective Mesoscopic and Macroscopic Elastic Properties of Cortical Bone," *Biomech. Model. Mechanobiol.*, **11**(6), pp. 883–901.
- [37] Granke, M., Grimal, Q., Saïed, A., Nauleau, P., Peyrin, F., and Laugier, P., 2011, "Change in Porosity is the Major Determinant of the Variation of Cortical Bone Elasticity at the Millimeter Scale in Aged Women," *Bone*, **49**(5), pp. 1020–1026.
- [38] Cai, X., Brenner, R., Peralta, L., Olivier, C., Gouttenoire, P.-J., Chappard, C., Peyrin, F., Cassereau, D., Laugier, P., and Grimal, Q., 2019, "Homogenization of Cortical Bone Reveals That the Organization and Shape of Pores Marginally Affect Elasticity," *J. R. Soc. Interface*, **16**(151), p. 20180911.
- [39] Sansalone, V., Naili, S., Bousson, V., Bergot, C., Peyrin, F., Zarka, J., Laredo, J. D., and Haiat, G., 2010, "Determination of the Heterogeneous Anisotropic Elastic Properties of Human Femoral Bone: From Nanoscopic to Organ Scale," *J. Biomech.*, **43**(10), pp. 1857–1863.
- [40] Aoubiza, B., Crolet, J. M., and Meunier, A., 1996, "On the Mechanical Characterization of Compact Bone Structure Using the Homogenization Theory," *J. Biomech.*, **29**(12), pp. 1539–1547.
- [41] Crolet, J. M., Aoubiza, B., and Meunier, A., 1993, "Compact Bone: Numerical Simulation of Mechanical Characteristics," *J. Biomech.*, **26**(6), pp. 677–687.
- [42] Katz, J. L., 1980, "Anisotropy of Young's Modulus of Bone," *Nature*, **283**(5742), pp. 106–107.
- [43] Sevostianov, I., and Kachanov, M., 2000, "Impact of the Porous Microstructure on the Overall Elastic Properties of the Osteonal Cortical Bone," *J. Biomech.*, **33**(7), pp. 881–888.
- [44] Salguero, L., Saadat, F., and Sevostianov, I., 2014, "Micromechanical Modeling of Elastic Properties of Cortical Bone Accounting for Anisotropy of Dense Tissue," *J. Biomech.*, **47**(13), pp. 3279–3287.
- [45] Parnell, W. J., and Grimal, Q., 2009, "The Influence of Mesoscale Porosity on Cortical Bone Anisotropy. Investigations Via Asymptotic Homogenization," *J. R. Soc. Interface*, **6**(30), pp. 97–109.
- [46] Scheiner, S., Pivonka, P., and Hellmich, C., 2016, "Poromicromechanics Reveals That Physiological Bone Strains Induce Osteocyte-Stimulating Lacunar Pressure," *Biomech. Model. Mechanobiol.*, **15**(1), pp. 9–28.
- [47] Fritsch, A., and Hellmich, C., 2007, "Universal' Microstructural Patterns in Cortical and Trabecular, Extracellular and Extravascular Bone Materials: Micromechanics-Based Prediction of Anisotropic Elasticity," *J. Theor. Biol.*, **244**(4), pp. 597–620.
- [48] Nikolov, S., and Raabe, D., 2008, "Hierarchical Modeling of the Elastic Properties of Bone at Submicron Scales: The Role of Extracellular Mineralization," *Biophys. J.*, **94**(11), pp. 4220–4232.
- [49] Hellmich, C., Barthélémy, J.-F., and Dormieux, L., 2004, "Mineral-Collagen Interactions in Elasticity of Bone Ultrastructure – A Continuum Micromechanics Approach," *Eur. J. Mech. A/Solids*, **23**(5), pp. 783–810.
- [50] Yoon, Y. J., and Cowin, S. C., 2008, "The Estimated Elastic Constants for a Single Bone Osteonal Lamella," *Biomech. Model. Mechanobiol.*, **7**(1), pp. 1–11.
- [51] Pidaparti, R., Chandran, A., Takano, Y., and Turner, C., 1996, "Bone Mineral Lies Mainly Outside Collagen Fibrils: Predictions of a Composite Model for Osteonal Bone," *J. Biomech.*, **29**(7), pp. 909–916.
- [52] Hellmich, C., and Ulm, F.-J., 2002, "Are Mineralized Tissues Open Crystal Foams Reinforced by Crosslinked Collagen?—Some Energy Arguments," *J. Biomech.*, **35**(9), pp. 1199–1212.
- [53] Hambli, R., and Barkaoui, A., 2012, "Physically Based 3D Finite Element Model of a Single Mineralized Collagen Microfibril," *J. Theor. Biol.*, **301**, pp. 28–41.
- [54] Siegmund, T., Allen, M. R., and Burr, D. B., 2008, "Failure of Mineralized Collagen Fibrils: Modeling the Role of Collagen Cross-Linking," *J. Biomech.*, **41**(7), pp. 1427–1435.
- [55] Morin, C., Vass, V., and Hellmich, C., 2017, "Micromechanics of Elastoplastic Porous Polycrystals: Theory, Algorithm, and Application to Osteonal Bone," *Int. J. Plasticity*, **91**, pp. 238–267.
- [56] Gailani, G., and Cowin, S., 2011, "Ramp Loading in Russian Doll Poroelasticity," *J. Mech. Phys. Solids*, **59**(1), pp. 103–120.
- [57] Sansalone, V., Bousson, V., Naili, S., Bergot, C., Peyrin, F., Laredo, J., and Haiat, G., 2012, "Anatomical Distribution of the Degree of Mineralization of Bone Tissue in Human Femoral Neck: Impact on Biomechanical Properties," *Bone*, **50**(4), pp. 876–884.
- [58] Sansalone, V., Bousson, V., Naili, S., Bergot, C., Peyrin, F., Laredo, J.-D., and Haiat, G., 2012, "Effects of the Axial Variations of Porosity and Mineralization on the Elastic Properties of the Human Femoral Neck," *Comput. Model. Eng. Sci.*, **87**(5), pp. 387–410.
- [59] Martínez-Reina, J., Domínguez, J., and García-Aznar, J. M., 2011, "Effect of Porosity and Mineral Content on the Elastic Constants of Cortical Bone: A Multiscale Approach," *Biomech. Model. Mechanobiol.*, **10**(3), pp. 309–322.
- [60] Racila, M., and Crolet, J. M., 2007, "Nano and Macro Structure of Cortical Bone: Numerical Investigations," *Mech. Adv. Mater. Struct.*, **14**(8), pp. 655–663.
- [61] Hamed, E., Novitskaya, E., Li, J., Chen, P.-Y., Jasiuk, I., and McKittrick, J., 2012, "Elastic Moduli of Untreated, Demineralized and Deproteinized Cortical Bone: Validation of a Theoretical Model of Bone as an Interpenetrating Composite Material," *Acta Biomater.*, **8**(3), pp. 1080–1092.
- [62] Hamed, E., Jasiuk, I., Yoo, A., Lee, Y. H., and Liszka, T., 2012, "Multi-Scale Modelling of Elastic Moduli of Trabecular Bone," *J. R. Soc. Interface*, **9**(72), pp. 1654–1673.
- [63] Athapreyangkul, A., Hoffman, M., and Pearce, G., 2021, "Effect of Geometrical Structure Variations on the Viscoelastic and Anisotropic Behaviour of Cortical Bone Using Multi-Scale Finite Element Modelling," *J. Mech. Behav. Biomed. Mater.*, **113**, p. 104153.
- [64] Vaughan, T., McCarthy, C., and McNamara, L., 2012, "A Three-Scale Finite Element Investigation Into the Effects of Tissue Mineralisation and Lamellar Organisation in Human Cortical and Trabecular Bone," *J. Mech. Behav. Biomed. Mater.*, **12**, pp. 50–62.
- [65] Deuerling, J. M., Yue, W., Espinoza Orías, A. A., and Roeder, R. K., 2009, "Specimen-Specific Multi-Scale Model for the Anisotropic Elastic Constants of Human Cortical Bone," *J. Biomech.*, **42**(13), pp. 2061–2067.
- [66] Baumann, A. P., Deuerling, J. M., Rudy, D. J., Niebur, G. L., and Roeder, R. K., 2012, "The Relative Influence of Apatite Crystal Orientations and Intracortical Porosity on the Elastic Anisotropy of Human Cortical Bone," *J. Biomech.*, **45**(16), pp. 2743–2749.
- [67] Gagliardi, D., Sansalone, V., Desceliers, C., and Naili, S., 2018, "Estimation of the Effective Bone-Elasticity Tensor Based on μ CT Imaging by a Stochastic Model. A Multi-Method Validation," *Eur. J. Mech. A/Solids*, **69**, pp. 147–167.
- [68] Orgel, J., Irving, T., Miller, A., and Wess, T., 2006, "Microfibrillar Structure of type I Collagen in Situ," *Proc. Natl. Acad. Sci.*, **103**(24), pp. 9001–9005.

- [69] Prostak, K., and Lees, S., 1996, "Visualization of Crystal-Matrix Structure. In Situ Demineralization of Mineralized turkey Leg Tendon and Bone," *Calcified Tissue Int.*, **59**(6), pp. 474–479.
- [70] Lees, S., Cleary, P. F., Heeley, J. D., and Garipey, E. L., 1979, "Distribution of Sonic Plesio-Velocity in a Compact Bone Sample," *J. Acoust. Soc. Am.*, **66**(3), pp. 641–646.
- [71] Jowsey, J., 1966, "Studies of Haversian Systems in Man and Some Animals," *J. Anatomy*, **100**(Pt 4), pp. 857–864.
- [72] Sinclair, C., Birch, H., Smith, R., and Goodship, A., 2014, *Skeletal Physiology: Responses to Exercise and Training*, Equine Sports Medicine and Surgery, W.B. Saunders, Elsevier, Amsterdam, The Netherlands, pp. 145–165.
- [73] Speirs, D. C. D., de Souza Neto, E. A., and Perić, D., 2008, "An Approach to the Mechanical Constitutive Modelling of Arterial Tissue Based on Homogenization and Optimization," *J. Biomech.*, **41**(12), pp. 2673–2680.
- [74] Morin, C., Avril, S., and Hellmich, C., 2018, "Non-Affine Fiber Kinematics in Arterial Mechanics: A Continuum Micromechanical Investigation," *ZAMM - J. Appl. Math. Mech./Z. Für Angew. Mathematik Und Mechanik*, **98**(12), pp. 2101–2121.
- [75] Spyrou, L. A., Brisard, S., and Danas, K., 2019, "Multiscale Modeling of Skeletal Muscle Tissues Based on Analytical and Numerical Homogenization," *J. Mech. Behav. Biomed. Mater.*, **92**, pp. 97–117.
- [76] Sree, V., Rausch, M., and Tepole, A., 2019, "Linking Microvascular Collapse to Tissue Hypoxia in a Multiscale Model of Pressure Ulcer Initiation," *Bio-mech. Model. Mechanobiol.*, **18**(6), pp. 1947–1964.
- [77] Gou, K., and Pence, T., 2016, "Hyperelastic Modeling of Swelling in Fibrous Soft Tissue With Application to Tracheal Angiodema," *J. Math. Biol.*, **72**(1–2), pp. 499–526.
- [78] Pissarenko, A., and Meyers, M., 2020, "The Materials Science of Skin: Analysis, Characterization, and Modeling," *Prog. Mater. Sci.*, **110**, p. 100634.
- [79] Xu, Y., Patnaik, S., Guo, X., Li, Z., Lo, W., Butler, R., Claude, A., Liu, Z., Zhang, G., Liao, J., Anderson, P., and Guan, J., 2014, "Cardiac Differentiation of Cardiosphere-Derived Cells in Scaffolds Mimicking Morphology of the Cardiac Extracellular Matrix," *Acta Biomater.*, **10**(8), pp. 3449–3462.
- [80] Huo, B., 2005, "An Inhomogeneous and Anisotropic Constitutive Model of Human Dentin," *J. Biomech.*, **38**(3), pp. 587–594.
- [81] Qin, Q.-H., and Swain, M., 2004, "A Micro-Mechanics Model of Dentin Mechanical Properties," *Biomaterials*, **25**(20), pp. 5081–5090.
- [82] Ma, S., Scheider, I., Yilmaz, E., Schneider, G., and Bargmann, S., 2018, *Bio-medical Technology – Modeling, Experiments and Simulation*, **84**, (Lecture Notes in Applied and Computational Mechanics), Springer International Publishing AG, Basel, Switzerland, chap., Multiscale experimental and computational investigation of nature's design principle of hierarchies in dental enamel.
- [83] Concha, F., Sarabia-Vallejos, M., and Hurtado, D., 2018, "Micromechanical Model of Lung Parenchyma Hyperelasticity," *J. Mech. Phys. Solids*, **112**, pp. 126–144.
- [84] Freed, A., Einstein, D., Carson, J., and Jacob, R., 2012, "Viscoelastic Model for Lung Parenchyma for Multi-Scale Modeling of Respiratory System, Phase II: Dodecahedral Micro-Model," Pacific Northwest National Lab, Richland, WA, Report No. PNNL-21287.
- [85] Sanz-Herrera, J. A., García-Aznar, J. M., and Doblaré, M. M., 2008, "Micro-Macro Numerical Modelling of Bone Regeneration in Tissue Engineering," *Comput. Methods Appl. Mech. Eng.*, **197**(33–40), pp. 3092–3107.
- [86] Sanz-Herrera, J. A., García-Aznar, J. M., and Doblaré, M., 2009, "On Scaffold Designing for Bone Regeneration: A Computational Multiscale Approach," *Acta Biomater.*, **5**(1), pp. 219–229.
- [87] Sanz-Herrera, J. A., García-Aznar, J. M., and Doblaré, M., 2009, "A Mathematical Approach to Bone Tissue Engineering," *Philos. Trans. R. Soc. London A: Math., Phys. Eng. Sci.*, **367**(1895), pp. 2055–2078.
- [88] Scheiner, S., Sinibaldi, R., Pichler, B., Komlev, V., Renghini, C., Vitale-Brovare, C., Rustichelli, F., and Hellmich, C., 2009, "Micromechanics of Bone Tissue-Engineering Scaffolds, Based on Resolution Error-Cleared Computer Tomography," *Biomaterials*, **30**(12), pp. 2411–2419.
- [89] Olivares, A., Marsal, E., Planell, J., and Lacroix, D., 2009, "Finite Element Study of Scaffold Architecture Design and Culture Conditions for Tissue Engineering," *Biomaterials*, **30**(30), pp. 6142–6149.
- [90] Jean, A., and Engelmayer, G., 2010, "Finite Element Analysis of an Accordion-Like Honeycomb Scaffold for Cardiac Tissue Engineering," *J. Biomech.*, **43**(15), pp. 3035–3043.
- [91] Ma, S., Scheider, I., and Bargmann, S., 2016, "Continuum Damage Modeling and Simulation of Hierarchical Dental Enamel," *Model. Simul. Mater. Sci. Eng.*, **24**(4), p. 045014.
- [92] van Rietbergen, B., Weinans, H., Huiskes, R., and Odgaard, A., 1995, "A New Method to Determine Trabecular Bone Elastic Properties and Loading Using Micromechanical Finite-Element Models," *J. Biomech.*, **28**(1), pp. 69–81.
- [93] Gross, T., Pahr, D. H., Peyrin, F., and Zysset, P. K., 2012, "Mineral Heterogeneity Has a Minor Influence on the Apparent Elastic Properties of Human Cancellous Bone: A SR μ CT-Based Finite Element Study," *Comput. Methods Biomech. Biomed. Eng.*, **15**(11), pp. 1137–1144.
- [94] Hambli, R., Katerchi, H., and Benhamou, C.-L., 2011, "Multiscale Methodology for Bone Remodelling Simulation Using Coupled Finite Element and Neural Network Computation," *Bio-mech. Model. Mechanobiol.*, **10**(1), pp. 133–145.
- [95] Grimal, Q., Raum, K., Gerisch, A., and Laugier, P., 2008, "Derivation of the Mesoscopic Elasticity Tensor of Cortical Bone From Quantitative Impedance Images at the Micron Scale," *Comput. Methods Biomech. Biomed. Eng.*, **11**(2), pp. 147–157.
- [96] Szlczak, K., Vass, V., Hasslinger, P., Jaroszewicz, J., Dejaco, A., Idaszek, J., Scheiner, S., Hellmich, C., and Swieszkowski, W., 2019, "X-Ray Physics-Based CT-to-Composition Conversion Applied to a Tissue Engineering Scaffold, Enabling Multiscale Simulation of Its Elastic Behavior," *Mater. Sci. Eng. C*, **95**, pp. 389–396.
- [97] Favata, A., 2012, "On the Kelvin Problem," *J. Elasticity*, **109**(2), pp. 189–204.
- [98] Lord Kelvin, W., 1848, "Note on the Integration of the Equations of Equilibrium of an Elastic Solid," *Cambridge Dublin Math. J.*, **3**, pp. 87–89.
- [99] Ting, T., and Lee, V.-G., 1997, "The Three-Dimensional Elastostatic Green's Function for General Anisotropic Linear Elastic Solids," *Q. J. Mech. Appl. Math.*, **50**(3), pp. 407–426.
- [100] Willis, J. R., 1977, "Bounds and Self-Consistent Estimates for the Overall Properties of Anisotropic Composites," *J. Mech. Phys. Solids*, **25**(3), pp. 185–202.
- [101] Kröner, E., 1977, "Bounds for Effective Elastic Moduli of Disordered Materials," *J. Mech. Phys. Solids*, **25**(2), pp. 137–155.
- [102] Walpole, L. J., 1966, "On Bounds for the Overall Elastic Moduli of Inhomogeneous Systems—I," *J. Mech. Phys. Solids*, **14**(3), pp. 151–162.
- [103] Lippmann, B. A., and Schwinger, J., 1950, "Variational Principles for Scattering Processes. I," *Phys. Rev.*, **79**(3), pp. 469–480.
- [104] Moulinec, H., and Suquet, P., 1998, "A Numerical Method for Computing the Overall Response of Nonlinear Composites With Complex Microstructure," *Comput. Methods Appl. Mech. Eng.*, **157**(1–2), pp. 69–94.
- [105] Brisard, S., and Dormieux, L., 2010, "FFT-Based Methods for the Mechanics of Composites: A General Variational Framework," *Comput. Mater. Sci.*, **49**(3), pp. 663–671.
- [106] Hashin, Z., 1963, *Theory of Mechanical Behavior of Heterogeneous Media*, Defense Technical Information Center. US Department of Defense University of Pennsylvania. Towne School of Civil and Mechanical Engineering, and United States. Office of Naval Research, Philadelphia, PA, Report No. AD0412503.
- [107] Eshelby, J., 1957, "The Determination of the Elastic Field of an Ellipsoidal Inclusion, and Related Problems," *Proc. R. Soc. London. Ser. A. Math. Phys. Sci.*, **241**, pp. 376–396.
- [108] Laws, N., 1977, "The Determination of Stress and Strain Concentrations at an Ellipsoidal Inclusion in an Anisotropic Material," *J. Elasticity*, **7**(1), pp. 91–97.
- [109] Einstein, A., 1905, "Eine Neue Bestimmung Der Moleküldimensionen [a New Determination of Molecule Dimensions]," Ph.D. thesis, University of Zurich, K. J. Wyss, Bern, Switzerland.
- [110] Mori, T., and Tanaka, K., 1973, "Average Stress in Matrix and Average Elastic Energy of Materials With Misfitting Inclusions," *Acta Metall.*, **21**(5), pp. 571–574.
- [111] Benveniste, Y., 1987, "A New Approach to the Application of Mori-Tanaka's Theory in Composite Materials," *Mech. Mater.*, **6**(2), pp. 147–157.
- [112] Kröner, E., 1958, "Berechnung Der Elastischen Konstanten Des Vielkristalls Aus Den Konstanten Des Einkristalls [Calculation of the Elastic Constants of the Polycrystal From the Constants of the Monocrystal]," *Z. Für Phys.*, **151**(4), pp. 504–518.
- [113] Hershey, A., 1954, "The Elasticity of an Isotropic Aggregate of Anisotropic Cubic Crystals," *ASME J. Appl. Mech.*, **21**(3), pp. 236–240.
- [114] Hill, R., 1965, "A Self-Consistent Mechanics of Composite Materials," *J. Mech. Phys. Solids*, **13**(4), pp. 213–222.
- [115] Hellmich, C., and Ulm, F.-J., 2002, "Micromechanical Model for Ultrastructural Stiffness of Mineralized Tissues," *J. Eng. Mech. (ASCE)*, **128**(8), pp. 898–908.
- [116] Laws, N., and McLaughlin, R., 1978, "Self-Consistent Estimates for the Viscoelastic Creep Compliances of Composite Materials," *Proc. R. Soc. London. Ser. A. Math. Phys. Sci.*, **359**(1697), pp. 251–273.
- [117] Eberhardsteiner, L., Hellmich, C., and Scheiner, S., 2014, "Layered Water in Crystal Interfaces as Source for Bone Viscoelasticity: Arguments From a Multiscale Approach," *Comput. Methods Biomech. Biomed. Eng.*, **17**(1), pp. 48–63.
- [118] Abate, J., and Valkó, P. P., 2004, "Multi-Precision Laplace Transform Inversion," *Int. J. Numer. Methods Eng.*, **60**(5), pp. 979–993.
- [119] Fritsch, A., Dormieux, L., and Hellmich, C., 2006, "Porous Polycrystals Built Up by Uniformly and Axisymmetrically Oriented Needles: Homogenization of Elastic Properties," *C. R. Méc.*, **334**(3), pp. 151–157.
- [120] Stroud, A. H., 1971, *Approximate Calculation of Multiple Integrals*, Prentice Hall, Englewood Cliffs, NJ.
- [121] Fritsch, A., Dormieux, L., Hellmich, C., and Sanahuja, J., 2009, "Mechanical Behavior of Hydroxyapatite Biomaterials: An Experimentally Validated Micromechanical Model for Elasticity and Strength," *J. Biomed. Mater. Res. Part A*, **88A**(1), pp. 149–161.
- [122] Dejaco, A., Komlev, V. S., Jaroszewicz, J., Swieszkowski, W., and Christian, C., 2012, "Micro CT-Based Multiscale Elasticity of Double-Porous (Pre-Cracked) Hydroxyapatite Granules for Regenerative Medicine," *J. Biomech.*, **45**(6), pp. 1068–1075.
- [123] Dejaco, A., Komlev, V. S., Jaroszewicz, J., Swieszkowski, W., and Hellmich, C., 2016, "Fracture Safety of Double-Porous Hydroxyapatite Biomaterials," *Bioinspired, Biomimetic Nanobiomater.*, **5**(1), pp. 24–36.
- [124] Sanahuja, J., Dormieux, L., Meille, S., Hellmich, C., and Fritsch, A., 2010, "Micromechanical Explanation of Elasticity and Strength of Gypsum: From Elongated Anisotropic Crystals to Isotropic Porous Polycrystals," *J. Eng. Mech. (ASCE)*, **136**(2), pp. 239–253.
- [125] Fritsch, A., Hellmich, C., and Young, P., 2013, "Micromechanics-Derived Scaling Relations for Porosity and Strength of Brittle Porous Polycrystals," *ASME J. Appl. Mech.*, **80**(2), p. 020905.
- [126] Levin, V., 1967, "Thermal Expansion Coefficient of Heterogeneous Materials," *Mekhanika Tverdogo Tela*, **2**(1), pp. 83–94.

- [127] Zaoui, A., 1997, *Structural Morphology and Constitutive Behavior of Micro-heterogeneous Materials* (CISM Courses and Lectures), Suquet, ed., Springer-Verlag, Wien New York, Vol. 377, pp. 291–347, Chap. 6.
- [128] Hellmich, C., and Ulm, F.-J., 2005, “Drained and Undrained Poroelastic Properties of Healthy and Pathological Bone: A Poro-Micromechanical Investigation,” *Transp. Porous Media*, **58**(3), pp. 243–268.
- [129] Hellmich, C., and Ulm, F.-J., 2005, “Microporodynamics of Bones: Prediction of the ‘Frenkel–Biot’ Slow Compressional Wave,” *J. Eng. Mech. (ASCE)*, **131**(9), pp. 918–927.
- [130] Hellmich, C., Celundova, D., and Ulm, F.-J., 2009, “Multiporoelasticity of Hierarchically Structured Materials: Micromechanical Foundations and Application to Bone,” *J. Eng. Mech. (ASCE)*, **135**(5), pp. 382–394.
- [131] Pichler, B., and Hellmich, C., 2010, “Estimation of Influence Tensors for Eigenstressed Multiphase Elastic Media With Nonaligned Inclusion Phases of Arbitrary Ellipsoidal Shape,” *J. Eng. Mech. (ASCE)*, **136**(8), pp. 1043–1053.
- [132] Dvorak, G. J., 1992, 1900, “Transformation Field Analysis of Inelastic Composite Materials,” *Proc. R. Soc. London. Ser. A: Math. Phys. Sci.*, **437**, pp. 311–327.
- [133] Dvorak, G. J., Bahei-El-Din, Y. A., and Wafa, A. M., 1994, “The Modeling of Inelastic Composite Materials With the Transformation Field Analysis,” *Model. Simul. Mater. Sci. Eng.*, **2**(3A), pp. 571–586.
- [134] Dvorak, G. J., and Benveniste, Y., 1992, “On Transformation Strains and Uniform Fields in Multiphase Elastic Media,” *Proc. R. Soc. London. Ser. A: Math. Phys. Sci.*, **437**, pp. 291–310.
- [135] Lubliner, J., 1990, *Plasticity Theory*, Macmillan, New York.
- [136] Morin, C., Hellmich, C., Nejim, Z., and Avril, S., 2021, “Fiber Rearrangement and Matrix Compression in Soft Tissues: Multiscale Hypoelasticity and Application to Tendon,” *Front. Bioeng. Biotechnol.*, **9**, p. 725047.
- [137] Rajagopal, K., and Srinivasa, A., 2007, “On the Response of Non-Dissipative Solids,” *Proc. R. Soc. A: Math., Phys. Eng. Sci.*, **463**(2078), pp. 357–367.
- [138] Rajagopal, K., and Srinivasa, A., 2009, “On a Class of Non-Dissipative Materials That Are Not Hyperelastic,” *Proc. R. Soc. A: Math., Phys. Eng. Sci.*, **465**(2102), pp. 493–500.
- [139] Chen, H., Zhao, X., Lu, X., and Kassab, G. S., 2013, “Non-Linear Micromechanics of Soft Tissues,” *Int. J. Non-Linear Mech.*, **56**, pp. 79–85.
- [140] Chen, H., Liu, Y., Zhao, X., Lanir, Y., and Kassab, G. S., 2011, “A Micromechanics Finite-Strain Constitutive Model of Fibrous Tissue,” *J. Mech. Phys. Solids*, **59**(9), pp. 1823–1837.
- [141] Chandran, P. L., and Barocas, V. H., 2006, “Affine Versus Non-Affine Fibril Kinematics in Collagen Networks: Theoretical Studies of Network Behavior,” *ASME J. Biomech. Eng.*, **128**(2), pp. 259–270.10
- [142] Stylianopoulos, T., and Barocas, V. H., 2007, “Multiscale, Structure-Based Modeling for the Elastic Mechanical Behavior of Arterial Walls,” *ASME J. Biomech. Eng.*, **129**(4), pp. 611–618.
- [143] Cyron, C. J., Müller, K. W., Bausch, A. R., and Wall, W. A., 2013, “Micromechanical Simulations of Biopolymer Networks With Finite Elements,” *J. Comput. Phys.*, **244**, pp. 236–251.
- [144] Picu, R. C., Deogekar, S., and Islam, M. R., 2018, “Poisson’s Contraction and Fiber Kinematics in Tissue: Insight From Collagen Network Simulations,” *ASME J. Biomech. Eng.*, **140**(2), p. 021002.
- [145] Popper, K. R., 1959, *The Logic of Scientific Discovery*, Basic Books, New York.
- [146] Popper, K. R., 1962, *Conjectures and Refutations: The Growth of Scientific Knowledge*, Routledge, New York.
- [147] Vass, V., Morin, C., Scheiner, S., and Hellmich, C., 2018, *Review of “Universal” Rules Governing Bone Composition, Organization, and Elasticity Across Organizational Hierarchies*, CISM Vol. 578, Springer, Cham, pp. 175–229.
- [148] Urist, M., DeLange, R., and Finerman, G., 1983, “Bone Cell Differentiation and Growth Factors,” *Science*, **220**(4598), pp. 680–686.
- [149] Gupta, H. S., Krauss, S., Kerschmitzki, M., Karunaratne, A., Dunlop, J., Barber, A., Boesecke, P., Funari, S., and Fratzl, P., 2013, “Intrafibrillar Plasticity Through Mineral/Collagen Sliding is the Dominant Mechanism for the Extreme Toughness of Antler Bone,” *J. Mech. Behav. Biomed. Mater.*, **28**, pp. 366–382.
- [150] Sansalone, V., Naili, S., and Desceliers, C., 2014, “A Stochastic Homogenization Approach to Estimate Bone Elastic Properties,” *C. R. Méc.*, **342**(5), pp. 326–333.
- [151] Gould, S. J., and Lewontin, R. C., 1979, “The Spandrels of San Marco and the Panglossian Paradigm: A Critique of the Adaptationist Programme,” *Proc. R. Soc. London. Ser. B. Biol. Sci.*, **205**(1161), pp. 581–598.
- [152] Riedl, R., 1975, *Die Ordnung Des Lebendigen. Systembedingungen Der Evolution [Order in Living Systems: A Systems Analysis of Evolution]*, Paul Perey, Hamburg/Berlin.
- [153] Gennisson, J.-L., Deffieux, T., Fink, M., and Tanter, M., 2013, “Ultrasound Elastography: Principles and Techniques,” *Diagn. Interv. Imaging*, **94**(5), pp. 487–495.
- [154] Carcione, J., 2015, *Wave Fields in Real Media: Wave Propagation in Anisotropic, Anelastic, Porous and Electromagnetic Media*, 3rd ed., Elsevier, Oxford, UK.
- [155] Kohlhauser, C., and Hellmich, C., 2013, “Ultrasonic Contact Pulse Transmission for Elastic Wave Velocity and Stiffness Determination: Influence of Specimen Geometry and Porosity,” *Eng. Struct.*, **47**, pp. 115–133.
- [156] Lees, S., Ahern, J. M., and Leonard, M., 1983, “Parameters Influencing the Sonic Velocity in Compact Calcified Tissues of Various Species,” *J. Acoust. Soc. Am.*, **74**(1), pp. 28–33.
- [157] Lees, S., Hanson, D. B., and Page, E. A., 1996, “Some Acoustical Properties of the Otic Bones of a Fin Whale,” *J. Acoust. Soc. Am.*, **99**(4), pp. 2421–2427.
- [158] Malandrino, A., Fritsch, A., Lahayne, O., Kropik, K., Redl, H., Noailly, J., Lacroix, D., and Hellmich, C., 2012, “Anisotropic Tissue Elasticity in Human Lumbar Vertebra, by Means of a Coupled Ultrasound-Micromechanics Approach,” *Mater. Lett.*, **78**, pp. 154–158.
- [159] Ashman, R. B., and Rho, J. Y., 1988, “Elastic Modulus of Trabecular Bone Material,” *J. Biomech.*, **21**(3), pp. 177–181.
- [160] Ashman, R. B., Cowin, S. C., Van Buskirk, W. C., and Rice, J. C., 1984, “A Continuous Wave Technique for the Measurement of the Elastic Properties of Cortical Bone,” *J. Biomech.*, **17**(5), pp. 349–361.
- [161] McCarthy, R. N., Jeffcott, L. B., and McCartney, R. N., 1990, “Ultrasound Speed in Equine Cortical Bone: Effects of Orientation, Density, Porosity and Temperature,” *J. Biomech.*, **23**(11), pp. 1139–1143.
- [162] Keaveny, T. M., Wachtel, E. F., Ford, C. M., and Hayes, W. C., 1994, “Differences Between the Tensile and Compressive Strengths of Bovine Tibial Trabecular Bone Depend on Modulus,” *J. Biomech.*, **27**(9), pp. 1137–1146.
- [163] Rho, J. Y., Hobatho, M. C., and Ashman, R. B., 1995, “Relations of Mechanical Properties to Density and CT Numbers in Human Bone,” *Med. Eng. Phys.*, **17**(5), pp. 347–355.
- [164] Turner, C. H., Cowin, S. C., Rho, J. Y., Ashman, R. B., and Rice, J. C., 1990, “The Fabric Dependence of the Orthotropic Elastic Constants of Cancellous Bone,” *J. Biomech.*, **23**(6), pp. 549–561.
- [165] Bilaniuk, N., and Wong, G. S. K., 1993, “Speed of Sound in Pure Water as a Function of Temperature,” *J. Acoust. Soc. Am.*, **93**(3), pp. 1609–1612.
- [166] Katz, J. L., and Ukrainick, K., 1971, “On the Anisotropic Elastic Properties of Hydroxyapatite,” *J. Biomech.*, **4**(3), pp. 221–227.
- [167] Cusack, S., and Miller, A., 1979, “Determination of the Elastic Constants of Collagen by Brillouin Light Scattering,” *J. Mol. Biol.*, **135**(1), pp. 39–51.
- [168] Morin, C., Hellmich, C., and Henis, P., 2013, “Fibrillar Structure and Elasticity of Hydrating Collagen: A Quantitative Multiscale Approach,” *J. Theor. Biol.*, **317**, pp. 384–393.
- [169] Meek, K. M., Fullwood, N. J., Cooke, P. H., Elliott, G. F., Maurice, D. M., Quantock, A. J., Wall, R. S., and Worthington, C. R., 1991, “Synchrotron X-Ray Diffraction Studies of the Cornea, With Implications for Stromal Hydration,” *Biophys. J.*, **60**(2), pp. 467–474.
- [170] Lees, S., and Heeley, J. D., 1981, “Density of a Sample Bovine Cortical Bone Matrix and Its Solid Constituent in Various Media,” *Calcified Tissue Int.*, **33**(1), pp. 499–504.
- [171] Cusack, S., and Lees, S., 1984, “Variation of Longitudinal Acoustic Velocity at Gigahertz Frequencies With Water Content in Rat-Tail Tendon Fibers,” *Biopolymers*, **23**(2), pp. 337–351.
- [172] Boal, D., 2012, *Mechanics of the Cell*, 2 ed., Cambridge University Press, Cambridge, UK.
- [173] Landau, L. D., and Lifshitz, E. M., 1958, *Statistical Physics*, Pergamon Press, London, UK.
- [174] Lodish, H., Berk, A., Zipursky, S. L., Matsudaira, P., Baltimore, D., and Darnell, J., 2000, *Molecular Cell Biology*, 4th ed., W. H. Freeman, New York.
- [175] Hofmann, H., Voss, T., Kühn, K., and Engel, J., 1984, “Localization of Flexible Sites in Thread-Like Molecules From Electron Micrographs: Comparison of Interstitial, Basement Membrane and Intima Collagens,” *J. Mol. Biol.*, **172**(3), pp. 325–343.
- [176] Kandola, D. K., et al., 2022, “Collagen Structure & Function,” *Proteopedia*, accessed July 18, 2022, https://proteopedia.org/wiki/index.php/Collagen_Structure_%26_Function
- [177] Bella, J., Eaton, M., Brodsky, B., and Berman, H. M., 1994, “Crystal and Molecular Structure of a Collagen-Like Peptide at 1.9 Å Resolution,” *Science*, **266**(5182), pp. 75–81.
- [178] Sasaki, N., and Odajima, S., 1996, “Stress-Strain Curve and Young’s Modulus of a Collagen Molecule as Determined by the X-Ray Diffraction Technique,” *J. Biomech.*, **29**(5), pp. 655–658.
- [179] Gentleman, E., Lay, A. N., Dickerson, D. A., Nauman, E. A., Livesay, G. A., and Dee, K. C., 2003, “Mechanical Characterization of Collagen Fibers and Scaffolds for Tissue Engineering,” *Biomaterials*, **24**(21), pp. 3805–3813.
- [180] Tai, K., Ulm, F.-J., and Ortiz, C., 2006, “Nanogranular Origins of the Strength of Bone,” *Nano Lett.*, **6**(11), pp. 2520–2525.
- [181] Salençon, J., 2001, *Handbook of Continuum Mechanics*, Springer-Verlag, Berlin Heidelberg.
- [182] Wang, T., and Feng, Z., 2005, “Dynamic Mechanical Properties of Cortical Bone: The Effect of Mineral Content,” *Mater. Lett.*, **59**(18), pp. 2277–2280.
- [183] Sasaki, N., Nakayama, Y., Yoshikawa, M., and Enyo, A., 1993, “Stress Relaxation Function of Bone and Bone Collagen,” *J. Biomech.*, **26**(12), pp. 1369–1376.
- [184] Sasaki, N., and Enyo, A., 1995, “Viscoelastic Properties of Bone as a Function of Water Content,” *J. Biomech.*, **28**(7), pp. 809–815.
- [185] Iyo, T., Maki, Y., Sasaki, N., and Nakata, M., 2004, “Anisotropic Viscoelastic Properties of Cortical Bone,” *J. Biomech.*, **37**(9), pp. 1433–1437.
- [186] Shahidi, M., Pichler, B., and Hellmich, C., 2014, “Viscous Interfaces as Source for Material Creep: A Continuum Micromechanics Approach,” *Eur. J. Mech. - A/Solids*, **45**, pp. 41–58.
- [187] Shahidi, M., Pichler, B., and Hellmich, C., 2016, “How Interface Size, Density, and Viscosity Affect Creep and Relaxation Functions of Matrix-Interface Composites: A Micromechanical Study,” *Acta Mech.*, **227**(1), pp. 229–252.
- [188] Luczynski, K. W., Steiger-Thirsfeld, A., Bernardi, J., Eberhardsteiner, J., and Hellmich, C., 2015, “Extracellular Bone Matrix Exhibits Hardening Elastoplasticity and More Than Double Cortical Strength: Evidence From Homogeneous Compression of Non-Tapered Single Micron-Sized Pillars Welded to a Rigid Substrate,” *J. Mech. Behav. Biomed. Mater.*, **52**, pp. 51–62.

- [189] Akao, M., Aoki, H., and Kato, K., 1981, "Mechanical Properties of Sintered Hydroxyapatite for Prosthetic Applications," *J. Mater. Sci.*, **16**(3), pp. 809–812.
- [190] Shareef, M. Y., Messer, P. F., and van Noort, R., 1993, "Fabrication, Characterization and Fracture Study of a Machinable Hydroxyapatite Ceramic," *Biomaterials*, **14**(1), pp. 69–75.
- [191] Schwiedrzik, J., Raghavan, R., Bürki, A., LeNader, V., Wolfram, U., Michler, J., and Zysset, P., 2014, "In Situ Micropillar Compression Reveals Superior Strength and Ductility but an Absence of Damage in Lamellar Bone," *Nat. Mater.*, **13**(7), pp. 740–747.
- [192] Schwiedrzik, J., Taylor, A., Casari, D., Wolfram, U., Zysset, P., and Michler, J., 2017, "Nanoscale Deformation Mechanisms and Yield Properties of Hydrated Bone Extracellular Matrix," *Acta Biomater.*, **60**, pp. 302–314.
- [193] Bigley, R. F., Griffin, L. V., Christensen, L., and Vandenbosch, R., 2006, "Osteon Interfacial Strength and Histomorphometry of Equine Cortical Bone," *J. Biomech.*, **39**(9), pp. 1629–1640.
- [194] Burstein, A. H., Currey, J. D., Frankel, V. H., and Reilly, D. T., 1972, "The Ultimate Properties of Bone Tissue: The Effects of Yielding," *J. Biomech.*, **5**(1), pp. 35–44.
- [195] Burstein, A. H., Zika, J. M., Heiple, K. G., and Klein, L., 1975, "Contribution of Collagen and Mineral to the Elastic-Plastic Properties of Bone," *J. Bone Jt. Surg. – Am. Vol.*, **57**(7), pp. 956–961.
- [196] Burstein, A. H., Reilly, D. T., and Martens, M., 1976, "Aging of Bone Tissue: Mechanical Properties," *J. Bone Jt. Surg. – Am. Vol.*, **58**(1), pp. 82–86.
- [197] Cezayirlioglu, H., Bahniuk, E., Davy, D. T., and Heiple, K. G., 1985, "Anisotropic Yield Behavior of Bone Under Combined Axial Force and Torque," *J. Biomech.*, **18**(1), pp. 61–69.
- [198] Currey, J. D., 1959, "Differences in the Tensile Strength of Bone of Different Histological Types," *J. Anatomy*, **93**(1), pp. 87–95.
- [199] Currey, J. D., 1975, "The Effects of Strain Rate, Reconstruction and Mineral Content on Some Mechanical Properties of Bovine Bone," *J. Biomech.*, **8**(1), pp. 81–86.
- [200] Currey, J. D., 1990, "Physical Characteristics Affecting the Tensile Failure Properties of Compact Bone," *J. Biomech.*, **23**(8), pp. 837–844.
- [201] Currey, J. D., 2004, "Tensile Yield in Compact Bone is Determined by Strain, Post-Yield Behaviour by Mineral Content," *J. Biomech.*, **37**(4), pp. 549–556.
- [202] Dickenson, R., Hutton, W., and Stott, J., 1981, "The Mechanical Properties of Bone in Osteoporosis," *J. Bone Jt. Surg. – British Vol.*, **63-B**(2), pp. 233–238.
- [203] Hellmich, C., Müllner, H., and Kohlhauser, C., 2006, "Mechanical (Triaxial) Tests on Biological Materials and Biomaterials," Network of Excellence 'Knowledge-based Multicomponent Materials for Durable and Safe Performance - KMM-NoE', sponsored by the European Commission, TU Wien, Vienna, Austria, Report No. DNRT3-1.2-3.
- [204] Kotha, S. P., and Guzelsu, N., 2002, "Modeling the Tensile Mechanical Behavior of Bone Along the Longitudinal Direction," *J. Theor. Biol.*, **219**(2), pp. 269–279.
- [205] Lee, S. C., Coan, B. S., and Bouxsein, M. L., 1997, "Tibial Ultrasound Velocity Measured in Situ Predicts the Material Properties of Tibial Cortical Bone," *Bone*, **21**(1), pp. 119–125.
- [206] Martin, R. B., and Ishida, J., 1989, "The Relative Effects of Collagen Fiber Orientation, Porosity, Density, and Mineralization on Bone Strength," *J. Biomech.*, **22**(5), pp. 419–426.
- [207] McCalden, R. W., McGeough, J. A., Barker, M. B., and Court-Brown, C. M., 1993, "Age-Related Changes in the Tensile Properties of Cortical Bone. The Relative Importance of Changes in Porosity, Mineralization, and Microstructure," *J. Bone Joint Surgery – Am. Vol.*, **75**(8), pp. 1193–1205.
- [208] Reilly, D. T., Burstein, A. H., and Frankel, V. H., 1974, "The Elastic Modulus for Bone," *J. Biomech.*, **7**(3), pp. 271–275.
- [209] Reilly, D. T., and Burstein, A. H., 1975, "The Elastic and Ultimate Properties of Compact Bone Tissue," *J. Biomech.*, **8**(6), pp. 393–405.
- [210] Riggs, C. M., Vaughan, L. C., Evans, G. P., Lanyon, L. E., and Boyde, A., 1993, "Mechanical Implications of Collagen Fibre Orientation in Cortical Bone of the Equine Radius," *Anat. Embryol.*, **187**(3), pp. 239–248.
- [211] Sedlin, E. D., and Hirsch, C., 1966, "Factors Affecting the Determination of the Physical Properties of Femoral Cortical Bone," *Acta Orthop. Scand.*, **37**(1), pp. 29–48.
- [212] Lees, S., 1987, "Considerations Regarding the Structure of the Mammalian Mineralized Osteoid From Viewpoint of the Generalized Packing Model," *Connective Tissue Res.*, **16**(4), pp. 281–303.
- [213] Bonar, L. C., Lees, S., and Mook, H. A., 1985, "Neutron Diffraction Studies of Collagen in Fully Mineralized Bone," *J. Mol. Biol.*, **181**(2), pp. 265–270.
- [214] Lees, S., Bonar, L. C., and Mook, H. A., 1984, "A Study of Dense Mineralized Tissue by Neutron Diffraction," *Int. J. Biol. Macromol.*, **6**(6), pp. 321–326.
- [215] Lees, S., 1986, "Water Content in Type I Collagen Tissues Calculated From the Generalized Packing Model," *Int. J. Biol. Macromol.*, **8**(2), pp. 66–72.
- [216] Lees, S., and Mook, H. A., 1986, "Equatorial Diffraction Spacing as a Function of Water Content in Fully Mineralized Cow Bone Determined by Neutron Diffraction," *Calcified Tissue Int.*, **39**(4), pp. 291–292.
- [217] Lees, S., and Probst, K., 1988, "The Locus of Mineral Crystallites in Bone," *Connective Tissue Res.*, **18**(1), pp. 41–54.
- [218] Lees, S., 2003, "Mineralization of type I Collagen," *Biophys. J.*, **85**(1), pp. 204–207.
- [219] Biltz, R., and Pellegrino, E., 1969, "The Chemical Anatomy of Bone," *J. Bone Jt. Surg. – Ser. A*, **51**(3), pp. 456–466.
- [220] Burns, C., 1929, "The Effect of the Continued Ingestion of Mineral Acid on Growth of Body and Bone and on the Composition of Bone and of the Soft Tissues," *Biochem. J.*, **23**(5), pp. 860–867.
- [221] Gong, J., Arnold, J., and Cohn, S., 1964, "Composition of Trabecular and Cortical Bone," *Anatomical Rec.*, **149**(3), pp. 325–331.
- [222] Hammett, F., 1925, "A Biochemical Study of Bone Growth. I. Changes in the Ash, Organic Matter and Water During Growth (Mus Norvegicus Albinus)," *J. Biol. Chem.*, **64**(2), pp. 409–428.
- [223] Lees, S., Heeley, J., and Cleary, P., 1979, "A Study of Some Properties of a Sample of Bovine Cortical Bone Using Ultrasound," *Calcified Tissue Int.*, **29**(1), pp. 107–117.
- [224] Lees, S., and Page, E., 1992, "A Study of Some Properties of Mineralized turkey Leg," *Connective Tissue Res.*, **28**(4), pp. 263–287.
- [225] Zelaya-Lainez, L., Kariem, H., Nischkauer, W., Limbeck, A., and Hellmich, C., 2020, "Variances" and "in-Variances" in Hierarchical Porosity and Composition, Across Femoral Tissues From Cow, Horse, Ostrich, Emu, Pig, Rabbit, and Frog," *Mater. Sci. Eng.: C*, **117**, p. 111234.
- [226] Hellmich, C., and Ulm, F.-J., 2003, "Average Hydroxyapatite Concentration is Uniform in the Extracellular Ultrastructure of Mineralized Tissues: Evidence at the 1–10- μ m Scale," *Biomech. Model. Mechanobiol.*, **2**(1), pp. 21–36.
- [227] Vuong, J., and Hellmich, C., 2011, "Bone Fibrillogenesis and Mineralization: Quantitative Analysis and Implications for Tissue Elasticity," *J. Theor. Biol.*, **287**, pp. 115–130.
- [228] Morin, C., and Hellmich, C., 2013, "Mineralization-Driven Bone Tissue Evolution Follows From Fluid-to-Solid Phase Transformations in Closed Thermodynamic Systems," *J. Theor. Biol.*, **335**, pp. 185–197.
- [229] Schneider, P., Stauber, M., Voide, R., Stapanoni, M., Donahue, L. R., and Müller, R., 2007, "Ultrastructural Properties in Cortical Bone Vary Greatly in Two Inbred Strains of Mice as Assessed by Synchrotron Light Based Micro- and Nano-ct," *J. Bone Miner. Res.*, **22**(10), pp. 1557–1570.
- [230] Kurfürst, A., Henits, P., Morin, C., Abdalrahman, T., and Hellmich, C., 2018, "Bone Ultrastructure as Composite of Aligned Mineralized Collagen Fibrils Embedded Into a Porous Polycrystalline Matrix: Confirmation by Computational Electrodynamics," *Front. Phys.*, **6**(125), pp. 1–20.
- [231] Blanchard, R., Morin, C., Malandrino, A., Vella, A., Sant, Z., and Hellmich, C., 2016, "Patient-Specific Fracture Risk Assessment of Vertebrae: A Multi-scale Approach Coupling X-Ray Physics and Continuum Micromechanics," *Int. J. Numer. Methods Biomed. Eng.*, **32**(9), p. e02760.
- [232] Hellmich, C., Kober, C., and Erdmann, B., 2008, "Micromechanics-Based Conversion of CT Data Into Anisotropic Elasticity Tensors, Applied to FE Simulations of a Mandible," *Ann. Biomed. Eng.*, **36**(1), pp. 108–122.
- [233] Yosibash, Z., Trabelsi, N., and Hellmich, C., 2008, "Subject-Specific p-FE Analysis of the Proximal Femur Utilizing Micromechanics-Based Material Properties," *Int. J. Multiscale Comput. Eng.*, **6**(5), pp. 483–498.
- [234] Crawley, E. O., Evans, W. D., and Owen, G. M., 1988, "A Theoretical Analysis of the Accuracy of Single-Energy CT Bone-Mineral Measurements," *Phys. Med. Biol.*, **33**(10), pp. 1113–1127.
- [235] Jackson, D. F., and Hawkes, D. J., 1981, "X-Ray Attenuation Coefficients of Elements and Mixtures," *Phys. Rep.*, **70**(3), pp. 169–233.
- [236] Boivin, G., and Meunier, P. J., 2002, "The Degree of Mineralization of Bone Tissue Measured by Computerized Quantitative Contact Microradiography," *Calcified Tissue Int.*, **70**(6), pp. 503–511.
- [237] Roschger, P., Gupta, H. S., Berzlanovich, A., Ittner, G., Dempster, D. W., Fratzl, P., Cosman, F., Parisien, M., Lindsay, R., Nieves, J. W., and Klaushofer, K., 2003, "Constant Mineralization Density Distribution in Cancellous Human Bone," *Bone*, **32**(3), pp. 316–323.
- [238] Akko, O., Polyakova-Akkus, A., Adar, F., and Schaffler, M. B., 2003, "Aging of Microstructural Compartments in Human Compact Bone," *J. Bone Miner. Res.*, **18**(6), pp. 1012–1019.
- [239] Bossy, E., Talmant, M., Peyrin, F., Akrou, L., Cloetens, P., and Laugier, P., 2004, "An In Vitro Study of the Ultrasonic Axial Transmission Technique at the Radius: 1-MHz Velocity Measurements Are Sensitive to Both Mineralization and Intracortical Porosity," *J. Bone Miner. Res.*, **19**(9), pp. 1548–1556.
- [240] Cheng, X. G., Nicholson, P. H., Boonen, S., Lowet, G., Brys, P., Aerssens, J., Van der Perre, G., and Dequeker, J., 1997, "Prediction of Vertebral Strength In Vitro by Spinal Bone Densitometry and Calcaneal Ultrasound," *J. Bone Miner. Res.*, **12**(10), pp. 1721–1728.
- [241] Perilli, E., Briggs, A. M., Kantor, S., Codrington, J., Wark, J. D., Parkinson, I. H., and Fazzalari, N. L., 2012, "Failure Strength of Human Vertebrae: Prediction Using Bone Mineral Density Measured by DXA and Bone Volume by micro-CT," *Bone*, **50**(6), pp. 1416–1425.
- [242] Crawford, R. P., Rosenberg, W. S., and Keaveny, T. M., 2003, "Quantitative Computed Tomography-Based Finite Element Models of the Human Lumbar Vertebral Body: Effect of Element Size on Stiffness, Damage, and Fracture Strength Predictions," *ASME J. Biomech. Eng.*, **125**(4), pp. 434–438.
- [243] McBroom, R. J., Hayes, W. C., Edwards, W. T., Goldberg, R. P., and White, A. A., 1985, "Prediction of Vertebral Body Compressive Fracture Using Quantitative Computed Tomography," *J. Bone Joint Surgery. Am. Vol.*, **67**(8), pp. 1206–1214.
- [244] Gatt, C. J., Jr., Hosea, T. M., Palumbo, R. C., and Zawadzky, J. P., 1997, "Impact Loading of the Lumbar Spine During Football Blocking," *Am. J. Sports Med.*, **25**(3), pp. 317–321.
- [245] Blanchard, R., Dejaco, A., Bongaers, E., and Hellmich, C., 2013, "Intravoxel Bone Micromechanics for microCT-Based Finite Element Simulations," *J. Biomech.*, **46**(15), pp. 2710–2721.
- [246] Yosibash, Z., Tal, D., and Trabelsi, N., 2010, "Predicting the Yield of the Proximal Femur Using High-Order Finite-Element Analysis With Inhomogeneous Orthotropic Material Properties," *Philos. Trans. R. Soc. A: Math., Phys. Eng. Sci.*, **368**(1920), pp. 2707–2723.

- [247] Kober, C., Kjeller, G., Hellmich, C., Sader, R., and Berg, B.-I., 2019, "Mandibular Biomechanics After Marginal Resection: Correspondences of Simulated Volumetric Strain and Skeletal Resorption," *J. Biomech.*, **95**, p. 109320.
- [248] Czenek, A., Blanchard, R., Dejaco, A., Sigurjónsson, O. E., Gissur, O., Gargiulo, P., and Hellmich, C., 2014, "Quantitative Intravoxel Analysis of microCT-Scanned Resorbing Ceramic Biomaterials—Perspectives for Computer-Aided Biomaterial Design," *J. Mater. Res.*, **29**(23), pp. 2757–2772.
- [249] Carter, D. R., Beaupré, G., Giori, N. J., and Helms, J. A., 1998, "Mechanobiology of Skeletal Regeneration," *Clinical Orthopaedics Relat. Res.*, **355**, pp. S41–S55.
- [250] van der Meulen, M. C. H., and Huiskes, R., 2002, "Why Mechanobiology?: a Survey Article," *J. Biomech.*, **35**(4), pp. 401–414.
- [251] Eyckmans, J., Boudou, T., Yu, X., and Chen, C. S., 2011, "A Hitchhiker's Guide to Mechanobiology," *Dev. Cell*, **21**(1), pp. 35–47.
- [252] Tyler, W. J., 2012, "The Mechanobiology of Brain Function," *Nat. Rev. Neurosci.*, **13**(12), pp. 867–878.
- [253] Jansen, K. A., Donato, D. M., Balcioglu, H. E., Schmidt, T., Danen, E. H. J., and Koenderink, G. H., 2015, "A Guide to Mechanobiology: Where Biology and Physics Meet," *Biochim. Biophys. Acta (BBA) - Mol. Cell Res.*, **1853**(11), pp. 3043–3052.
- [254] Scheiner, S., Pivonka, P., and Hellmich, C., 2013, "Coupling Systems Biology With Multiscale Mechanics, for Computer Simulations of Bone Remodeling," *Comput. Methods Appl. Mech. Eng.*, **254**, pp. 181–196.
- [255] Pastrama, M. I., Scheiner, S., Pivonka, P., and Hellmich, C., 2018, "A Mathematical Multiscale Model of Bone Remodeling, Accounting for Pore Space-Specific Mechanosensation," *Bone*, **107**, pp. 208–221.
- [256] Estermann, S. J., and Scheiner, S., 2018, "Multiscale Modeling Provides Differentiated Insights to Fluid Flow-Driven Stimulation of Bone Cellular Activities," *Front. Phys.*, **6**, p. 76.
- [257] Pivonka, P., Buenzli, P., Scheiner, S., Hellmich, C., and Dunstan, C., 2013, "The Influence of Bone Surface Availability in Bone Remodelling – A Mathematical Model Including Coupled Geometrical and Biomechanical Regulations of Bone Cells," *Eng. Struct.*, **47**, pp. 134–147.
- [258] Lerebours, C., Buenzli, P. R., Scheiner, S., and Pivonka, P., 2016, "A Multiscale Mechanobiological Model of Bone Remodelling Predicts Site-Specific Bone Loss in the Femur During Osteoporosis and Mechanical Disuse," *Bio-mech. Model. Mechanobiol.*, **15**(1), pp. 43–67.
- [259] Adachi, T., Osako, Y., Tanaka, M., Hojo, M., and Hollister, S. J., 2006, "Framework for Optimal Design of Porous Scaffold Microstructure by Computational Simulation of Bone Regeneration," *Biomaterials*, **27**(21), pp. 3964–3972.
- [260] Sturm, S., Zhou, S., Mai, Y.-W., and Li, Q., 2010, "On Stiffness of Scaffolds for Bone Tissue Engineering – A Numerical Study," *J. Biomech.*, **43**(9), pp. 1738–1744.
- [261] Imamura, K., Ozawa, H., Hiraide, T., Shibasaki, Y., Fukuhara, T., Takahashi, N., and Suda, T., 1990, "Continuously Applied Compressive Pressure Induces Bone Resorption by a Mechanism Involving Prostaglandin E2 Synthesis," *J. Cellular Physiol.*, **144**(2), pp. 222–228.
- [262] Ozawa, H., Imamura, K., Abe, E., Takahashi, N., Hiraide, T., Shibasaki, Y., Fukuhara, T., and Suda, T., 1990, "Effect of a Continuously Applied Compressive Pressure on Mouse Osteoblast-Like Cells (MC3T3-E1) In Vitro," *J. Cellular Physiol.*, **142**(1), pp. 177–185.
- [263] Klein-Nulend, J., and van der Plas, A., 2008, "Sensitivity of Osteocytes to Biomechanical Stress In Vitro. FASEB. 1995; 9(5): 441–5. Vatsa A, Breuls RG, Semeins CM, Salmon PL, Smit TH, Klein-Nulend J. Osteocyte Morphology in Fibula and Calvaria—is There a Role for Mechanosensing," *Bone*, **43**(3), pp. 452–458.
- [264] Roelofsens, J., Klein-Nulend, J., and Burger, E. H., 1995, "Mechanical Stimulation by Intermittent Hydrostatic Compression Promotes Bone-Specific Gene Expression In Vitro," *J. Biomech.*, **28**(12), pp. 1493–1503.
- [265] Brighton, C. T., Fisher, J. R., Jr., Levine, S. E., Corsetti, J. R., Reilly, T., Landsman, A. S., Williams, J. L., and Thibault, L. E., 1996, "The Biochemical Pathway Mediating the Proliferative Response of Bone Cells to a Mechanical Stimulus," *J. Bone Joint Surgery. Am. Volume*, **78**(9), pp. 1337–1347.
- [266] Vergne, L., Meunier, A., Meunier, A., and Sedel, L., 1996, "A New Apparatus for Studying the Effect of Hydrostatic Pressure on Cells in Culture," *Cytotechnology*, **21**(1), pp. 21–30.
- [267] Rubin, J., Biskobing, D., Fan, X., Rubin, C., McLeod, K., and Taylor, W. R., 1997, "Pressure Regulates Osteoclast Formation and MCSF Expression in Marrow Culture," *J. Cellular Physiol.*, **170**(1), pp. 81–87.
- [268] Nagatomi, J., Arulananandam, B. P., Metzger, D. W., Meunier, A., and Bizios, R., 2001, "Frequency- and Duration-Dependent Effects of Cyclic Pressure on Select Bone Cell Functions," *Tissue Eng.*, **7**(6), pp. 717–728.
- [269] Nagatomi, J., Arulananandam, B. P., Metzger, D. W., Meunier, A., and Bizios, R., 2002, "Effects of Cyclic Pressure on Bone Marrow Cell Cultures," *ASME J. Biomech. Eng.*, **124**(3), pp. 308–314.
- [270] Nagatomi, J., Arulananandam, B. P., Metzger, D. W., Meunier, A., and Bizios, R., 2003, "Cyclic Pressure Affects Osteoblast Functions Pertinent to Osteogenesis," *Ann. Biomed. Eng.*, **31**(8), pp. 917–923.
- [271] Takai, E., Mauck, R. L., Hung, C. T., and Guo, X. E., 2004, "Osteocyte Viability and Regulation of Osteoblast Function in a 3D Trabecular Bone Explant Under Dynamic Hydrostatic Pressure," *J. Bone Miner. Res.*, **19**(9), pp. 1403–1410.
- [272] Maul, T. M., Hamilton, D. W., Nieponice, A., Soletti, L., and Vorp, D. A., 2007, "A New Experimental System for the Extended Application of Cyclic Hydrostatic Pressure to Cell Culture," *ASME J. Biomech. Eng.*, **129**(1), pp. 110–116.06
- [273] Gardinier, J. D., Majumdar, S., Duncan, R. L., and Wang, L., 2009, "Cyclic Hydraulic Pressure and Fluid Flow Differentially Modulate Cytoskeleton Reorganization in mc3t3 Osteoblasts," *Cellular Mol. Bioeng.*, **2**(1), pp. 133–143.
- [274] Liu, J., Zhao, Z., Li, J., Zou, L., Shuler, C., Zou, Y., Huang, X., Li, M., and Wang, J., 2009, "Hydrostatic Pressures Promote Initial Osteodifferentiation With ERK1/2 Not p38 MAPK Signaling Involved," *J. Cellular Biochem.*, **107**(2), pp. 224–232.
- [275] Liu, C., Zhao, Y., Cheung, W.-Y., Gandhi, R., Wang, L., and You, L., 2010, "Effects of Cyclic Hydraulic Pressure on Osteocytes," *Bone*, **46**(5), pp. 1449–1456.
- [276] Rottmar, M., Ackerknecht, S., Wick, P., and Maniura-Weber, K., 2011, "A High Throughput System for Long Term Application of Intermittent Cyclic Hydrostatic Pressure on Cells in Culture," *ASME J. Biomechanical Eng.*, **133**(2), p. 024502.
- [277] Henstock, J. R., Rotherham, M., Rose, J., and El Haj, A., 2013, "Cyclic Hydrostatic Pressure Stimulates Enhanced Bone Development in the Foetal Chick Femur In Vitro," *Bone*, **53**(2), pp. 468–477.
- [278] Kojic, M., Filipovic, N., Stojanovic, B., and Kojic, N., 2008, *Computer Modeling in Bioengineering: Theoretical Background, Examples and Software*, Wiley and Sons, Hoboken, NJ.
- [279] Filipovic, N., Zivic, M., Obradovic, M., Djukic, T., Markovic, Z., and Rosic, M., 2014, "Numerical and Experimental LDL Transport Through Arterial Wall," *Microfluid. Nanofluid.*, **16**(3), pp. 455–464.
- [280] Lin, S.-J., Jan, K.-M., Schuessler, G., Weinbaum, S., and Chien, S., 1988, "Enhanced Macromolecular Permeability of Aortic Endothelial Cells in Association With Mitosis," *Atherosclerosis*, **73**(2–3), pp. 223–232.
- [281] Wolfgram, S., 1986, "Cellular Automaton Fluids I: Basic Theory," *J. Stat. Phys.*, **45**(3–4), pp. 471–526.
- [282] Filipovic, N., Haber, S., Kojic, M., and Tsuda, A., 2008, "Dissipative Particle Dynamics Simulation of Flow Generated by Two Rotating Concentric Cylinders: Ii. lateral Dissipative and Random Forces," *J. Phys. D: Appl. Phys.*, **41**(3), p. 035504.
- [283] Filipovic, N., Kojic, M., and Tsuda, A., 2008, "Modelling Thrombosis Using Dissipative Particle Dynamics Method," *Philos. Trans. R. Soc. A: Math., Phys. Eng. Sci.*, **366**(1879), pp. 3265–3279.
- [284] Filipovic, N., Ravnic, D., Kojic, M., Mentzer, S. J., Haber, S., and Tsuda, A., 2008, "Interactions of Blood Cell Constituents: Experimental Investigation and Computational Modeling by Discrete Particle Dynamics Algorithm," *Microvascular Res.*, **75**(2), pp. 279–284.
- [285] Kojic, M., Filipovic, N., and Tsuda, A., 2008, "A Mesoscopic Bridging Scale Method for Fluids and Coupling Dissipative Particle Dynamics With Continuum Finite Element Method," *Comput. Methods Appl. Mech. Eng.*, **197**(6–8), pp. 821–833.
- [286] Rodriguez, M. L., McGarry, P. J., and Sniadecki, N. J., 2013, "Review on Cell Mechanics: Experimental and Modeling Approaches," *ASME Appl. Mech. Rev.*, **65**(6), p. 060801.
- [287] Krieg, M., Fläschner, G., Alsteens, D., Gaub, B. M., Roos, W. H., Wuite, G. J. L., Gaub, H. E., Gerber, C., Dufrene, Y. F., and Müller, D. J., 2019, "Atomic Force Microscopy-Based Mechanobiology," *Nat. Rev. Phys.*, **1**(1), pp. 41–57.
- [288] Radmacher, M., 2007, "Studying the Mechanics of Cellular Processes by Atomic Force Microscopy," *Methods in Cell Biol.*, **83**, pp. 347–372.
- [289] Costa, K., and Yin, F., 1999, "Analysis of Indentation: Implications for Measuring Mechanical Properties With Atomic Force Microscopy," *ASME J. Biomech. Eng.*, **121**(5), pp. 462–471.
- [290] Moreno-Flores, S., Benitez, R., Vivanco, M., and Toca-Herrera, J., 2010, "Stress Relaxation and Creep on Living Cells With the Atomic Force Microscope: A Means to Calculate Elastic Moduli and Viscosities of Cell Components," *Nanotechnology*, **21**(44), p. 445101.
- [291] Cartagena-Rivera, A., Logue, J., Waterman, C., and Chadwick, R., 2016, "Actomyosin Cortical Mechanical Properties in Nonadherent Cells Determined by Atomic Force Microscopy," *Biophys. J.*, **110**(11), pp. 2528–2539.
- [292] Rheinlaender, J., Dimitracopoulos, A., Wallmeyer, B., Kronenberg, N., Chalut, K., Gather, M., Betz, T., Charras, G., and Franze, K., 2020, "Cortical Cell Stiffness is Independent of Substrate Mechanics," *Nat. Mater.*, **19**(9), pp. 1019–1025.
- [293] Tang, G., Galluzzi, M., Zhang, B., Shen, Y. L., and Stadler, F. J., 2019, "Biomechanical Heterogeneity of Living Cells: Comparison Between Atomic Force Microscopy and Finite Element Simulation," *Langmuir: ACS J. Surf. Coll.*, **35**(23), pp. 7578–7587.
- [294] Desprat, N., Richert, A., Simeon, J., and Asnacios, A., 2005, "Creep Function of a Single Living Cell," *Biophys. J.*, **88**(3), pp. 2224–2233.
- [295] Vaziri, A., Xue, Z., Kamm, R. D., and Kaazempur Mofrad, M. R., 2007, "A Computational Study on Power-Law Rheology of Soft Glassy Materials With Application to Cell Mechanics," *Comput. Methods Appl. Mech. Eng.*, **196**(31–32), pp. 2965–2971.
- [296] Mofrad, M. R. K., 2009, "Rheology of the Cytoskeleton," *Annu. Rev. Fluid Mech.*, **41**(1), pp. 433–453.
- [297] Cai, P. G., Mizutani, Y., Tsuchiya, M., Maloney, J. M., Fabry, B., Van Vliet, K. J., and Okajima, T., 2013, "Quantifying Cell-to-Cell Variation in Power-Law Rheology," *Biophys. J.*, **105**(5), pp. 1093–1102.
- [298] Patrício, P., Leal, C. R., Duarte, J., and Januário, C., 2015, "Rheology of the Cytoskeleton as a Fractal Network," *Phys. Rev. E*, **92**(4), p. 040702.
- [299] Cardamone, L., Laio, A., Torre, V., Shahapure, R., and DeSimone, A., 2011, "Cytoskeletal Actin Networks in Motile Cells Are Critically Self-Organized Systems Synchronized by Mechanical Interactions," *Proc. Natl. Acad. Sci.*, **108**(34), pp. 13978–13983.

- [300] Gupta, M., Sarangi, B. R., Deschamps, J., Nematbakhsh, Y., Callan-Jones, A., Margadant, F., Mége, R.-M., Lim, C. T., Voituriez, R., and Ladoux, B., 2015, "Adaptive Rheology and Ordering of Cell Cytoskeleton Govern Matrix Rigidity Sensing," *Nat. Commun.*, **6**(1), p. 7525.
- [301] Fallqvist, B., and Kroon, M., 2016, "Constitutive Modelling of Composite Biopolymer Networks," *J. Theor. Biol.*, **395**, pp. 51–61.
- [302] Gong, B., Wei, X., Qian, J., and Lin, Y., 2019, "Modeling and Simulations of the Dynamic Behaviors of Actin-Based Cytoskeletal Networks," *ACS Biomater. Sci. Eng.*, **5**(8), pp. 3720–3734.
- [303] Hafner, A. E., Krausser, J., and Šarić, A., 2019, "Minimal Coarse-Grained Models for Molecular Self-Organisation in Biology," *Curr. Opin. Struct. Biol.*, **58**, pp. 43–52.
- [304] Freedman, S. L., Banerjee, S., Hocky, G. M., and Dinner, A. R., 2017, "A Versatile Framework for Simulating the Dynamic Mechanical Structure of Cytoskeletal Networks," *Biophys. J.*, **113**(2), pp. 448–460.
- [305] Pešek, J., Baerts, P., Smeets, B., Maes, C., and Ramon, H., 2016, "Mathematical Model Suitable for Efficient Simulation of Thin Semi-Flexible Polymers in Complex Environments," *Soft Mat.*, **12**(14), pp. 3360–3387.
- [306] Duman, O., Isele-Holder, R. E., Elgeti, J., and Gompper, G., 2018, "Collective Dynamics of Self-Propelled Semiflexible Filaments," *Soft Mat.*, **14**(22), pp. 4483–4494.
- [307] Müller, K. W., Cyron, C. J., and Wall, W. A., 2015, "Computational Analysis of Morphologies and Phase Transitions of Cross-Linked, Semi-Flexible Polymer Networks," *Proc. R. Soc. A: Math., Phys. Eng. Sci.*, **471**(2182), p. 20150332.
- [308] Nie, W., Wei, M.-T., Ou-Yang, H. D., Jedlicka, S. S., and Vavylonis, D., 2015, "Formation of Contractile Networks and Fibers in the Medial Cell Cortex Through Myosin-ii Turnover, Contraction, and Stress-Stabilization," *Cytoskeleton*, **72**(1), pp. 29–46.
- [309] Bidone, T. C., Jung, W., Maruri, D., Borau, C., Kamm, R. D., and Kim, T., 2017, "Morphological Transformation and Force Generation of Active Cytoskeletal Networks," *PLoS Comput. Biol.*, **13**(1), p. e1005277.
- [310] Miller, C. J., Harris, D., Weaver, R., Ermentrout, G., and Davidson, L. A., 2018, "Emergent Mechanics of Actomyosin Drive Punctuated Contractions and Shape Network Morphology in the Cell Cortex," *PLoS Comput. Biol.*, **14**(9), p. e1006344.
- [311] Wollrab, V., Belmonte, J. M., Baldauf, L., Leptin, M., Nédélec, F., and Koenderink, G. H., 2018, "Polarity Sorting Drives Remodeling of Actin-Myosin Networks," *J. Cell Sci.*, **132**(4), p. jcs219717.
- [312] Soares e Silva, M., Stuhmann, B., Betz, T., and Koenderink, G., 2014, "Time-Resolved Microreology of Actively Remodeling Actomyosin Networks," *New J. Phys.*, **16**(7), p. 075010.
- [313] Marchetti, M. C., Joanny, J. F., Ramaswamy, S., Liverpool, T. B., Prost, J., Rao, M., and Simha, R. A., 2013, "Hydrodynamics of Soft Active Matter," *Rev. Mod. Phys.*, **85**(3), pp. 1143–1189.
- [314] Prost, J., Jülicher, F., and Joanny, J. F., 2015, "Active Gel Physics," *Nat. Phys.*, **11**(2), pp. 111–117.
- [315] Alt, W., and Dembo, M., 1999, "Cytoplasm Dynamics and Cell Motion: Two-Phase Flow Models," *Math. Biosci.*, **156**(1–2), pp. 207–228.
- [316] Jülicher, F., Grill, S. W., and Salbreux, G., 2018, "Hydrodynamic Theory of Active Matter," *Rep. Prog. Phys.*, **81**(7), p. 076601.
- [317] Mogilner, A., and Manhart, A., 2018, "Intracellular Fluid Mechanics: Coupling Cytoplasmic Flow With Active Cytoskeletal Gel," *Annu. Rev. Fluid Mech.*, **50**(1), pp. 347–370.
- [318] Reymann, A.-C., Staniscia, F., Erzberger, A., Salbreux, G., and Grill, S. W., 2016, "Cortical Flow Aligns Actin Filaments to Form a Furrow," *eLife*, **5**, p. e17807.
- [319] Pimpale, L. G., Middelkoop, T. C., Mietke, A., and Grill, S. W., 2020, "Cell Lineage-Dependent Chiral Actomyosin Flows Drive Cellular Rearrangements in Early *Caenorhabditis elegans* Development," *eLife*, **9**, p. e54930.
- [320] Giomi, L., and DeSimone, A., 2014, "Spontaneous Division and Motility in Active Nematic Droplets," *Phys. Rev. Lett.*, **112**(14), p. 147802.
- [321] Strychalski, W., and Guy, R. D., 2016, "Intracellular Pressure Dynamics in Blebbing Cells," *Biophys. J.*, **110**(5), pp. 1168–1179.
- [322] Heck, T., Vargas, D., Smeets, B., Ramon, H., Van Liedekerke, P., and Van Oosterwyck, H., 2020, "The Role of Actin Protrusion Dynamics in Cell Migration Through a Degradable Viscoelastic Extracellular Matrix: Insights From a Computational Model," *PLOS Comput. Biol.*, **16**(1), p. e1007250.
- [323] Soiné, J., Brand, C., Stricker, J., Oakes, P., Gardel, M., and Schwarz, U., 2015, "Model-Based Traction Force Microscopy Reveals Differential Tension in Cellular Actin Bundles," *PLOS Comput. Biol.*, **11**(3), p. e1004076.
- [324] Germain, P., 1973, "The Method of Virtual Power in Continuum Mechanics. Part 2: Microstructure," *Soc. Ind. Appl. Math.: J. Appl. Math.*, **25**(3), pp. 556–575.
- [325] Kalliauer, J., Kahl, G., Scheiner, S., and Hellmich, C., 2020, "A New Approach to the Mechanics of DNA: Atoms-to-Beam Homogenization," *J. Mech. Phys. Solids*, **143**, p. 104040.
- [326] Kothari, P., Johnson, C., Sandone, C., Iglesias, P. A., and Robinson, D. N., 2019, "How the Mechanobiome Drives Cell Behavior, Viewed Through the Lens of Control Theory," *J. Cell Sci.*, **132**(17), p. jcs234476.
- [327] Pérez, A., Luque, F. J., and Orozco, M., 2012, "Frontiers in Molecular Dynamics Simulations of DNA," *Accounts Chem. Res.*, **45**(2), pp. 196–205.
- [328] Pradhan, S., Katti, D., and Katti, K., 2011, "Steered Molecular Dynamics Study of Mechanical Response of Full Length and Short Collagen Molecules," *J. Nanomechanics Micromech.*, **1**(3), pp. 104–110.
- [329] Streeter, I., and de Leeuw, N. H., 2011, "A Molecular Dynamics Study of the Interprotein Interactions in Collagen Fibrils," *Soft Mat.*, **7**(7), pp. 3373–3382.